

**DETERMINING THE THERMAL EFFECTS OF CHANNELS ON POROUS HEAT
SINKS UNDER FORCED CONVECTION CONDITIONS WITH NANOFLUID: AN
EXPERIMENTAL AND NUMERICAL STUDY**

Christopher Welsford

Bachelor of Mechanical Engineering, Ryerson University, 2018

A thesis presented to Ryerson University

in partial fulfilment of the requirements for the degree of Master of Applied Science in the
program of Mechanical Engineering

Toronto, Ontario, Canada, 2019

©Christopher Welsford, 2019

Author's Declaration

I hereby declare that I am the sole author of this thesis. This is a true copy of the thesis, including any required final revisions, as accepted by my examiners.

I authorize Ryerson University to lend this thesis to other institutions or individuals for the purpose of scholarly research

I further authorize Ryerson University to reproduce this thesis by photocopying or by other means, in total or in part, at the request of other institutions or individuals for the purpose of scholarly research.

I understand that my thesis may be made electronically available to the public.

Acknowledgements

The author would like to thank Ryerson University and the National Science and Engineering Research Council of Canada for their continued funding and support which made the following possible.

Determining the Thermal Effects of Channels on Porous Heat Sinks Under Forced Convection Conditions with Nanofluid, Christopher Welsford, Master Applied Science, Ryerson University, 2019

Abstract

The present study determines the effects which foam metals and Nanofluid have on the performance of a simulated CPU. The present study employs γAl_2O_3 -water Nanofluid and 6061-T6 Aluminum foam metal with a porosity of 0.91 and permeability of 40 pores per linear inch formed in bulk media and porously filled channels. The concentrations evaluated are 0.1%, 0.3%, and 0.6% by volume. The study shall consider both original empirical results and numerical results obtained from COMSOL Multiphysics, showing good agreement with a maximum error of 4.3%. The present study. When considering the average Nusselt number as the representation of the strength of the heat transfer mechanism, and as such ignoring pumping requirements, it is shown that the use of porously filled channels interacting with 0.6% Nanofluid produces the most effective combination. However, when pumping power is relevant, a combination of bulk porous media interacting with 0.3% Nanofluid is observed. The results obtained herein can be applied to the cooling of electronics, or any other system wherein a general inward heat flux is applied.

Table of Contents

Abstract	iv
List of Figures	vii
List of Tables	ix
1 Introduction.....	1
1.1 Fluid Transport Phenomena	1
1.1.1 Porous Media	2
1.1.2 Nanofluids.....	4
1.2 Thermal Transport Phenomena.....	7
1.2.1 Porous Media	7
1.2.2 Nanofluids.....	17
2 Experimental Procedure and Apparatus.....	22
2.1 Apparatus and Procedure	22
2.2 Uncertainty and Error Analysis	26
3 Finite Element Formulations and Boundary Conditions	28
3.1 Governing Equations	28
3.2 Boundary Conditions and Domains	30
3.3 Meshing and Finite Element Scheme	33
4 Discussion and Analysis of Results	35
4.1 Effect of Flow Rate on System Performance.....	36

4.2	Effect of Heat Flux on System Performance	44
4.3	Effect of Nanoparticle Concentration on System Performance	49
4.4	Effect of Channels on System Performance	53
4.5	Applications of Results	57
5	Concluding Remarks and Future Work	58
5.1	Conclusions.....	58
5.2	Future Work.....	59
	References.....	61

List of Figures

Figure 1: Experimental Test Section.....	23
Figure 2: Cross-Section of Test Area.....	23
Figure 3: Schematic of Apparatus.....	23
Figure 4: Domains and Boundary Conditions for (a) Purely Porous Model and (b) Porous Channel Model	31
Figure 5: Mesh Sensitivity Study.....	34
Figure 6: Meshing Scheme for (a) Bulk Media and (b) Porously Filled Channels	34
Figure 7: Temperature Distributions at Constant Heat Flux for (a) Bulk Media (b) Porously Filled Channels.....	37
Figure 8: Index of Performance for Bulk and Channel Geometries	39
Figure 9: Temperature Distributions for 0.3% and 0.6% interacting with (a) Bulk Media and (b) Porously Filled Channels	41
Figure 10: Index of Performance by Flow Rate for 0.3% and 0.6% Nanoparticle Concentration	44
Figure 11: Temperature Distribution for (a) Bulk Media and (b) Porously Filled Channels Interacting with 0.1% Nanofluid.....	45
Figure 12: Temperature Distribution for (a) Bulk Media and (b) Porously Filled Channels Interacting with 0.3% Nanofluid.....	47
Figure 13: Temperature Distribution for (a) Bulk Media and (b) Porously Filled Channels Interacting with 0.6% Nanofluid.....	47
Figure 14: Temperature Distributions for (a) Bulk Porous Media and (b) Porously Filled Channels for All Nanofluid Concentrations	50
Figure 15: Average Nusselt Number Based on Nanofluid Concentration.....	51

Figure 16: Effect of Nanofluid Concentration on Index of Performance 52

Figure 17: Velocity Profiles for (a) Bulk Media and (b) Porously Filled Channels 54

Figure 18: Velocity Profile Through Centre of the Test Sample 55

Figure 19: Plane Temperature Distribution for (a) Bulk Media and (b) Porously Filled Channels
..... 56

List of Tables

Table 1: Nanofluid Properties Obtained from Ho et. al. (2008-2013).....	29
Table 2: Numerical System Domains	31
Table 3: Finite Element Meshing Scheme	33
Table 4: Numerical Pressure Drop and Mean Velocity by Flow Rate for 0.1% Nanofluid	38
Table 5: Average Nusselt Number and Fanning Friction Factor for 0.1% Nanofluid at Constant Heat Flux with Varied Flow Rate	39
Table 6: Numerical Pressure Drop and Mean Velocity by Flow Rate for 0.3% Nanofluid	42
Table 7: Numerical Pressure Drop and Mean Velocity by Flow Rate for 0.6% Nanofluid	42
Table 8: Average Nusselt Number and Fanning Friction Factor for 0.3% Nanofluid.....	43
Table 9: Average Nusselt Number and Fanning Friction Factor for 0.6% Nanofluid.....	43
Table 10: Average Nusselt Number for Varied Heat Flux	48
Table 11: Average Nusselt Number for Porously Filled Channels.....	48
Table 12: Average Nusselt Number and Index of Performance for Bulk Media and Porously Filled Channels.....	53

1 Introduction

The objective of the following is the study of the relationship between several parameters operating within a fluid mechanics system. Particularly the study shall evaluate experimentally and compare numerically the effects of the following system parameters: heat flux, flow rate, Nanofluid concentration, and the insertion of foam metal into machined microchannels. By furthering our understanding of the effects of these parameters the engineering community will be better able to make design decisions where porous media and Nanofluid systems are involved. As well, this experimental work will contribute much needed empirical data to the scientific community.

To begin it is important to discuss the deviations from conventional fluid mechanics which necessitate this work. The first of these deviations is the use of porous media. The particular medium which will be considered for the following is known commonly as metal or cellular foam. Specifically, we shall be looking at high-porosity open-celled foam metals. As the name suggests, unlike conventional porous media the foam metals have an open-celled geometry. This means that the porosity of the material is not derived as a result of spacing between particles but rather is controlled by the size of the ligaments which generate the structure of the medium. The second deviation exists as a result of the introduction of Nanoparticles into a base carrying fluid, thus, creating a Nanofluid. The Nanofluids can be loosely defined as a multiphase fluid system consisting of two phases. The liquid phase which acts as the carrying fluid, and a solid phase which is composed of the Nanoparticles. In order to be considered a Nanofluid the particles in question must be homogeneously distributed and to the order of less than 100 nm in their agglomerated form. The exact details which drive the fluid phenomena with respect to both of these deviations shall be discussed in detail below.

1.1 Fluid Transport Phenomena

The following section intends to analyze on a subject based approach the development for fluid flow properties and characteristics of both Nanofluids and porous media.

1.1.1 Porous Media

The introduction of porous media for use in thermal augmentation has been of interest to researchers for over 100 years. Now, while it is of more importance to look at most recent developments in this area, it does help to fundamentally understand the origins of these modern derivations and models.

Flow through porous media was originally modeled as a series of *pore tubes* in 1856 by Henry Darcy [1]. While the primary topic of the work was the distribution of water through a city, its management, and its sanitation, Darcy also proposed a model for fluid flow through sand. The model suggested that the spaces between the particulates could be modeled as a series of tubes, later becoming known as *pore tubes*. This seminal work represents the first real attempt to model fluid flow through porous media. It was of course later learned that this model had many failings, but it allowed for a baseline from which further development could be made. In this work Darcy, suggests a series of equations which come to be known as *Darcy's Law*. While these equations are still widely used today for the modeling of hydrodynamic systems, they yielded room for improvement.

1.1.1.1 Numerical Modeling

In more recent years, the advent of computers has changed how researchers and engineers approach the modeling of fluid systems. New techniques including finite element methods and more advanced statistical models have allowed for a dramatic increase in the precision with which one can predict the behaviour of fluids within a system.

Kopanidis et. al. (2010) performed a three-dimensional flow study on foam metals on the pore scale [2]. The study employed the use of a tetrahedral volume mesh, Navier-Stokes flow, and the energy equation with two different pore densities and varied temperature and fluid conditions. It was observed in the study that the use of three-dimensional ligaments deviated greatly from conventional approximations. The authors believed that the differentiating factors between the three-dimensional Navier-stokes model and the conventional studies was the consideration of entry effects. The three-dimensional model offered a more realistic picture of fluid behaviour within the entry region while many existing approximations regard it as negligible. Further, the authors

observed that the heat transfer through the ligaments of the porous foam was not consistent with conventional models.

Ranut et. al. (2014) performed a microtomographic study on computational fluid dynamics and heat transfer within aluminum metal foams [3]. The authors observed the existence of several irregularities in the geometry of the samples from what is typically modeled. Particularly, it was noted that the roughness of the porous samples varied consistently with the linear pore density of the samples. Further, the authors were able to validate the use of Darcy-Forchheimer flow through porous media using their realistic model of the sample. Lastly, it is worth noting that the experimenters were able to validate their results against previously performed experiments. This result is of particular importance as the Darcy-Forchheimer flow model is widely used in the modeling of porous media and its validation allows for direction in future study.

In 2015 Diani et. al. investigated numerically the pressure drop and heat transfer through metal foam [4]. The approach used non-destructive three-dimensional X-ray tomography to develop a model for numerical simulation. Using this three-dimensional slicing technique in combination with commercial finite elements software, the authors observed that predictions for pressure drop fell within five percent of experimental results. The use of this highly accurate technique is widely accepted as a valid approach for the modeling of complex geometries within fluid systems. However, it is not often employed as a result of its high infrastructural costs.

Xu et. al. (2018) performed a study, again, on the behaviour of fluids in three-dimensions on the pore scale within foam metals [5]. In this study a sufficiently low flow rate was used to allow the authors to directly apply Navier-Stokes flow to the model. The objective was to determine the aeroacoustics of the metal foam, However, the results presented on permeability and pressure drop are what is of interest here. The authors employed an approach of circular reduction to model the cells, this differs from Kopanidis et. al. [2] and likely better represents the actual geometry of a single pore. The study revealed interesting symmetric behaviour of vortices within a pore cell. As well the authors observed that the pressure drop within the cell cannot be considered as a directly linear function with respect to Reynolds number. It was observed that with small variation of the Reynolds number there was large disparity in the behaviour of the fluid.

1.1.1.2 Experimental Study

In the pursuit of complex fluid mechanics, the collection of experimental data proves to be of great importance, as often complex systems are too difficult to map analytically. As such the empirical correlations established through experimentation offer an important and irrefutable base line for comparison. The establishment of this data allows for the verification of modeled accuracy where an analytical solution would normally be employed.

In 2014 Dukhan et. al. conducted a study on the hydrodynamics of metal foams, ranging from the pre-Darcy region through turbulent flow [6]. They observed that as the flow regime changed the effective permeability and corresponding Forchheimer coefficient changed as well. Further they noted that using the square-root of the permeability offered good correlation to the pressure drop observed from experimentation. This information is of particular value as the pressure drop through the foam is a controlling factor in the performance of the foam metal as a heat sink overall.

Dyga et. al. (2017) experimentally evaluated the behaviour of multi-phase, gas-liquid, fluid flow through foam metal filled channels [7]. The authors observed that fluid flow parameters through porous filled channels are largely a function of the properties of the fluids being used. This is contrary to what is observed in heat transfer within porous media, where the properties of the foam metal are the primary drivers in thermal enhancement. This implies then that the properties, both geometric and material, play a smaller part in effecting the flow through the system. The authors do however note that the properties of the foam greatly impact the pressure drop.

1.1.2 Nanofluids

The approach to modeling Nanofluids operating within systems is a widely debated and disputed topic. Among the most common approaches is the assumption that the Nanofluid behaves as any other Newtonian fluid. However, while this approach is accepted it is also widely argued that the only accurate method for the modelling of Nanofluids is as a multiphase mixture. However, these multiphase mixture models themselves face issues around computational demands, and what approach is appropriate for the scale of the suspended Nanoparticles themselves. For example, it is frequently debated as to which body forces play an important role in modeling Nanofluids accurately. Some argue that factors such as thermophoresis and shear lift forces do not play a substantial enough role for consideration.

1.1.2.1 Numerical Modeling

The use of numerical models when considering fluid flow and Nanofluids is broadly debated and discussed. Particularly a large centre of debate lies around how to simulate Nanofluids given current computational limitations. Ideally, one would be able to model each particle as it moved through the system, and, as such be able to get a more realistic estimation of what occurred within the multiphase mixture itself. However, as mentioned above such simulations are not widely possible due to computational limitations. As such, it is a much more common practice to utilize equivalency factors to model a modified conventional flow system (laminar, turbulent, etc.).

Ho et. al. (2008-2012) studied Numerically and experimentally the influence of fluid property uncertainty on Nanofluid modelling under various operating conditions [8] [9] [10] [11]. The study considered the use of Al_2O_3 Nanoparticles suspended in water with a concentration ranging from 0%-4% by volume. The properties obtained by Ho et. al. are used in the present study to model the Nanofluid.

Arefmanesh and Mahmoodi (2011) presented a study on the effects of uncertainty models on the viscosity of alumina-water Nanofluid [12]. The study focussed on mixed convection conditions within a square cavity with constant temperature at all walls with the bottom wall as the hottest. As well, the bottom plate had an induced constant velocity. The combination of this induced velocity and temperature gradient is what the authors employed to induce mixed convection. The solution technique employed to solve this problem was that of a finite volume approach. Ultimately, the authors observed that when considering the uncertainty of the viscosity of the Nanofluid, there exist two parameters which have the greatest influence, the Richardson number and the concentration of the employed Nanoparticles. Specifically, it is observed that as the volume fraction of the Nanoparticles is increased, so too is the uncertainty of the viscosity. Lastly, the authors note that when regarding systems with a high Richardson number, the Maiga's correlation tends to underestimate the average Nusselt number when compared to Brinkman's equations.

Sheikholeslami and Sadoughi (2017) studied the effects of magnetic field disturbances on the fluid properties of Nanoscale ferrofluids [13]. Particularly, the study considered the use of Fe_3O_4 -water Nanofluid. When considering only Nanofluid concentrations and its effects on the streamline of the fluids, it can be seen that the test containing only pure water has a more even distribution of

streamlines with an overall higher average velocity, while the Nanofluid has tighter contours with a lower average velocity. This effect is likely a result of the increased viscosity of the fluid within the system. When considering only Nanofluids and the effect of the magnetic radiation, it was observed that the use of radiation separated the streamlines and ultimately increased the average velocity of the system. This is likely as a result of the magnetic properties of the Nanoparticles employed and their tendency to move with respect to the source.

Etaig et. al. (2018) studied a newly developed model for the effective viscosity of Nanofluids [14]. The model proposes something similar to classical Nanofluid models wherein the viscosity is a function of the fraction of the concentration of the Nanofluid. After extensive literature review and mathematical manipulation, the authors present their model for Nanofluid effective viscosity as shown below.

$$\frac{\mu_{eff}}{\mu_f} = 1 + 5\phi + 80\phi^2 + 120\phi^3 \quad (1)$$

The authors note that this function for effective viscosity is a function of the base fluid and as such can be further manipulated given the empirical values of the particular system being studied. When developing the model, the authors further noted a maximum deviation of 5% during the expansion and refinement of the above used coefficients. After comparing the results with existing data, in the form of numerical theoretical and experimental results, the authors were able to observe good agreement across a range of flow rates temperatures and Nanofluid concentrations.

1.1.2.2 Experimental Study

As is the case with many fields of study, the amount of experimental results for fluidic behaviour of Nanofluids is limited as a function of cost. Due to the high cost to acquire or synthesize Nanofluids the amount of empirical data which is available is limited. Further, it is likely that the amount of research being done into Nano fluidics is even more limited as most of the interest surrounding Nanofluids looks at their use as thermal performance enhancers. This highly focussed interest has created a divide in the literature, relegating the study of fluid properties to an almost secondary task.

Soltani and Akbari (2016) conducted an experimental study on the effects of temperature and particle concentration on MgO-MWCNT/ethylene glycol hybrid nanofluid [15]. The study considered Nanofluid concentrations of 0.1%, 0.2%, 0.4%, 0.8%, and 1%. The authors were able to observe a nonlinear trend in the effect of increasing Nanofluid concentration on viscosity. Particularly they note that at lower concentrations the effect is notably less than that of higher concentrations. Overall the authors cite that they observed a total increase in viscosity by 168% when going from only the base fluid to a concentration of 1%. This significant increase in effective fluid dynamic viscosity is important to note for the development of technologies which may want to employ Nanofluids for practical applications. However, the authors do state that across all tested temperature ranges and concentrations the fluid did display Newtonian fluid behaviour.

Moldoveanu et. al. (2018) experimentally studied the viscosity of stabilized Al₂O₃ and TiO₂ Nanofluids as well as the hybridized fluid combining both of the above [16]. As is expected when considering viscosity in Nanofluids, the increase in Nanoparticle concentration resulted in an increase in the viscosity of the fluid. The authors demonstrated good agreement between the correlation presented within the paper and the experimental results, but poor agreement between other models which had been previously developed. Further, the authors demonstrated a larger increase in the viscosity of the alumina sample than the titania sample. Lastly, it is significant to note that for all tested cases the authors observed non-Newtonian behaviour. This implication challenges many of the previously established relationships which were assumed to be valid when simulating Nanofluids.

1.2 Thermal Transport Phenomena

The objective of this section is to introduce literature which has affected the modeling of various thermal properties of foam metals and Nanofluids with engineering applications. The following includes the modeling and representation of boundaries, as well as material parameters which are used in the modelling of foam metals.

1.2.1 Porous Media

The use of porous media for augmentation of thermal performance is becoming a widely discussed topic with respect to engineering applications. There exist several driving factors, such as high

surface area to volume ratio, which make these foam metals such favourable candidates for heat exchangers.

1.2.1.1 Numerical Modeling

As was observed in the modeling of fluid behaviour within porous media the use of recent computational technology had increased greatly the precision with which predictions can be made on the movement of energy through systems involving porous media.

Hsu et. al. in 1993 performed a study analyzing the effectiveness of a modified Zehner-Schlunder model for stagnant thermal conductivity within porous media [17]. The model proposes that the effective thermal conductivity of a particular metal foam is a function of the material and fluid properties, as well as the geometry of the medium. The study yields that the effective thermal conductivity can be expressed as:

$$\frac{k_e}{k_f} = \left[1 - \sqrt{1 - \phi} \right] + \frac{\sqrt{1 - \phi}}{\lambda} \left(1 - \frac{1}{(1 + \alpha B)^2} \right) + \frac{(2\sqrt{1 - \phi})}{[1 - \lambda B + (1 - \lambda)\alpha B]} \left(\frac{(1 - \lambda)(1 + \alpha)B}{[1 - \lambda B + (1 - \lambda)\alpha B]^2} \times \right. \\ \left. \ln \frac{1 + \alpha B}{(1 + \alpha)B\lambda} - \frac{B + 1 + 2\alpha B}{2(1 + \alpha B)^2} - \frac{B - 1}{[1 - \lambda B + (1 - \lambda)\alpha B](1 + \alpha B)} \right) \quad (2)$$

Where B is the shape factor, α is the deformed factor, λ is the ratio of fluid to solid thermal conductivity, $\frac{k_e}{k_f}$ is the dimensionless conductivity of the system, and ϕ is the porosity. Many approximations of a similar nature to this exist for a wide variety of porous media, including foam metals. While it is not pertinent to list all of such equations below it is worth noting that all found will take a similar form, where the deviation lies in the development of geometric factors.

Bhattacharya et. al. (2001) discussed further the thermophysical properties of highly porous metal foams [18]. The study aimed to determine the effective thermal conductivity, inertial coefficient, and permeability of the aforementioned metal foams. Ultimately, the researchers developed an analytical model for the thermal conductivity using a hexagonal geometry where the ligaments ran the perimeter of the pore, and the relatively massive junctions were represented with circular nodes. Both the analysis and experiment showed that the effective thermal conductivity and permeability of the foam metals were highly dependent on the porosity and the ratio of the cross-sections and the fibre. This further suggests that the geometry which is used in analytically

modeling the foam metals is crucial in order to ensure accuracy between simulation and experimentation.

Further extending the use of a ligament and node-based geometry, Boomsma et. al. (2001) studied the effective thermal conductivity of a three-dimensionally structured fluid-saturated metal foam [19]. The model proposed by Boomsma et. al. employed a tetrakaidekahedral unit cell with cylindrical ligaments and square cross-sections. The significance of this paper lies in the detailed decomposition of the porous cells which the author undertook. The geometry of the system is clearly described and defined. This allows subsequent researchers to be able to replicate and improve the accuracy of the model. This model was an improvement on its ancestral two-dimensional models, as it allowed for considerations across all directions of the pores complex surface. To minimize the computational demand the authors reduced and analogized the three-dimensional parameters into an overall one-dimensional model. As previously mentioned, this model still proved advantageous over existing models as it took into account the three-dimensional factors of the system. However, this model was proven to be in error. Dai et. al. (2010) presented a paper in which they corrected the geometric considerations of Boomsma et. al. (2001) and then continued to further extend the model [20]. Dai et. al. pointed out that in spite of certain errors the model would continue to display inaccuracy as a result of the author's neglect to consider the spatial orientation of the ligaments within a pore. Dai et. al. proposed that the inclusion of the ligament angle would help to mitigate the error of the widely volume fraction driven model which existed. As a response to the commentary made by Dai et. al. (2010), Boomsma et. al. (2011) rederived their geometric factors and presented a corrigendum to the scientific community with the corrected equations and plots [21].

Nield et. al. (2003) studied thermal development through a channel formed by two flat plates filled with porous media [22]. Most significantly the authors noted that the addition of a viscous dissipation term greatly influences the Nusselt number. This is significant as the Nusselt number is a valuable parameter in determining the effectiveness of a forced convection system as a heat sink. The large deviation in the Nusselt number with respect to viscous dissipation then implies that the dissipative effects must be considered when numerically simulating the system.

Kuznetsov et. al. (2009) conducted an analytical study on the convection characteristics of a rarefied gas flowing through porous media [23]. Both two flat plates and cylindrical flow. The

analysis considered both plates, or the wall of the cylinder, to be of constant heat flux. The study used the Brinkman equations to model the fluid within the system. In order to quantify and make comparison between the results the authors developed two coefficients for comparison. One for velocity slip and one for temperature slip. For the temperature slip coefficient, the authors observed a direct relationship to the Knudsen number. Whereas, for the velocity slip coefficient, it was observed that at high Darcy numbers the behaviour became too complex to model.

Hooman et. al. (2007) conducted a study on heat transfer and entropy generation in a rectangular duct with constant wall heat flux [24]. The study looked to improve understanding of how the Brinkman flow model could be used in cases where the flow parameters disallow the use of conventional Darcy equations. The authors applied an extended weight residuals method combined with a Galerkin approach to solve the aforementioned system of equations. As well, the authors observed a noticeable reduction in the systems Nusselt number when viscous dissipation was considered. Lastly, the authors state that the developed model is appropriate for use as a benchmarking tool when considering porous experimental systems.

Vijay et. al. (2018) studied numerically the thermal characteristics of foam metals based on a geometric model obtained from CT images [25]. Particularly, the study considered samples with linear pore densities between 10 PPI, and 30 PPI, and porosity between 79% and 87%. The study used CT images to develop a geometric model which was then homogeneously distributed as a continuous array of individual cells. These simplified continuous models were compared to actual geometric models which were also obtained through CT processes. This allowed the authors to evaluate the applicability of the simplified model for practical use. Ultimately, the authors observe that the use of the simplified *macroscopic* model succeeds at predicting the convective heat transfer mechanisms but fails at determining the diffusive behaviour. This leads the author to the conclusion that the use of both microscopic and macroscopic approaches must be employed in order to accurately model a system under real conditions. Further, the authors elude that this is likely a result of the inhomogeneous nature of the foam metals.

Xu et. al. (2018) studied numerically the thermal behaviour of gradient metal foams partially filling tubes under forced convection conditions [26]. For the purpose of this investigation the authors employed both Brinkman-Darcy and local thermal non-equilibrium models. The models in question were both compared to previously collected data for validation. Four foam samples were

considered, the linear pore density was represented as two numbers, where the first number represents the linear pore density at the wall, and the second represents the linear pore density towards the centre of the tube. The three samples were then 5 PPI-20 PPI, 20 PPI-5 PPI, 5 PPI-10 PPI, and 5 PPI-40 PPI. The authors observed that in the cases where the pore density increases from the inside out so too did the velocity of the fluid. The authors believe that this is likely as a result of varying flow resistance. As well it is worth noting that, the authors observed a decrease in Nusselt number as the linear pore density increased from the wall to the centre, and that the Nusselt number tended to be higher when the linear pore density decreased in radial direction towards the centre.

Gandomkar and Gray (2018) conducted a numerical study into the effects of thermal equilibrium and nonequilibrium models [27]. The results presented in the paper are then compared to previous work completed on the topic. While the stated goal of the authors to develop an analytical model, which removes the need for approximation was not fully validated or verified, the authors did state that the results obtained using the linear thermal non-equilibrium model influenced the temperature distribution. This suggests that the classical assumption of uniform temperature between solid and fluid phases may not be accurate for all systems.

Chen (2018) numerically analyzed the conjugate heat transfer between a fluid-saturated porous medium and a solid wall [28]. The author particularly looks at the use of a lattice Boltzmann method to address the complex nature of the conjugate heat transfer which exists between porous media and other sources. The results obtained were verified using three non-trivial sets of benchmark data. The author successfully demonstrated the ability of such lattice-Boltzmann approaches to complete the prediction. However, it was suggested that the model be better verified using experimental data and extended to include multiple relaxation time simulations.

Gong et. al. (2018) developed an approach to develop finned metal foam heat sinks with applications in electronics cooling [29]. The study presented the results as a function of fin spacing and foam size. The authors observed that although the pressure drop in the foam combined heat sink was lower so too was the thermal performance of the system. The authors believe that this is likely as a result of the decreased mainstream velocity caused by the foam. Ultimately, the authors observed that there did exist an optimal point at which the thermal performance including pumping power would be a maximum. The authors stated that at a dimensionless fin thickness ratio of 0.2

the system would experience optimal performance. Lastly, the authors make a note that the viscous effects induced by the porous media seem to not have substantial effects.

1.2.1.2 Experimental Study

Similarly, to what was observed with fluid flow through porous media the need for experimental data cannot be understated. While some researchers will conduct original empirical evidence collection to support their results, many rely on the use of previously completed collections. This has created somewhat of a hole in the literature where the experimental study of porous media has become somewhat ignored, and researchers continue to use repeatedly the same sets of data. However, there do exist several experiments which are worth noting.

Bhattacharya et. al. studied the effectiveness of metal foams interacting with fins to operate as heat sinks with electronics cooling applications [30]. The study analyzed the effectiveness of two different pore density samples (5 PPI and 20 PPI), under varying heat flux, flow rate and fin spacing. They showed successfully that the use of metal foams enhanced the thermal performance of finned heat sinks. However, they did qualify this assertion by stating that the enhancement was limited by situational constraints on the pumping power of the system. This stipulation was added as a result of the increased pressure drop across the heat sink.

Boomsma et. al. (2003) studied the effectiveness of compressed or compact metal foams with applications as high-performance heat exchangers [31]. The study compared one base sample of metallic 6061-T6 metal foam with several samples under various compression ratios. As well, the effects of the working fluid were analyzed, comparing water and water-glycol solution. It was shown that the compressed foam heat exchangers reduced thermal resistance in the simulated systems when compared to commercially available equipment. As well it was stated that due to a lower thermal capacitance of the glycol-water solution it was necessary to increase the volumetric flow-rate. This can be considered as a required increase in the work required by a pump to match the original heat-rate. Thus, it can also then be argued that the water was the favourable working fluid in the experiment.

Hetsroni et. al. (2004) preformed an experiment to determine the effectiveness of foam metals as heat syncs under forced convection conditions [32]. In the experiment a sample of 40 PPI 6061-T6 aluminum foam metal was used. The authors noted that with forced air convection from a fan,

the porous media was able to *easily* dissipate the required energy. Notably, they stated that an outward heat flux of 0.25 kW/cm^2 was observed. As well, the experimenters obtained a measured pressure drop of 20 bar/m. Ultimately, the authors state that the use of metal foams with applications in the cooling and dissipation of radiant and conductive energy even in sensitive applications, such as the cooling of laser transmission windows shows potential.

Zhao et. al. (2004) performed a more general study on the thermofluidic nature of porous media [33]. The study encompassed both numerical and experimental results including study on both the heat transfer properties and pressure distributions through the foam. Ultimately, this allowed the authors to develop and substantiate a model for heat transfer within the foam metals. The study looked at two major categories of foams based on the type of material used. One sample was composed of FeCrAlY and the other was an undisclosed copper alloy. For each of the materials size separate samples were prepared and labeled. Out of these six there were two samples of each 10, 30, and 60 PPI, further, for each linear pore density one of the two samples would have a nominal relative density of 5% and the other would be of 10%. The first step the experimenters took was the study of the morphological properties of the foam samples. This includes properties such as: actual relative density, permeability, and geometric pore scale quantities. From this initial study the researchers noted substantial deviation from the supplied values and the measured values. The experimenters were able to successfully measure the pressure drop and Nusselt number distributions of the aforementioned samples. Notably, they show that the copper sample substantially out performs the FeCrAlY samples. As well, the experimental data allowed the authors to demonstrate that their numerical predictions were accurate to what was occurring in reality. It was however noted that, the prediction did somewhat underestimate the Nusselt number when compared.

Noh et. al. (2006) performed a study on the effectiveness of porous media on the enhancement of thermal performance in an annular heat exchanger under non-Darcy flow conditions [34]. To conduct the experiment 3 10 PPI samples were used with varying permeability and ratios of radius. The experimenters were able to determine the effectiveness of the new heat sync through the measurement of both wall temperatures and temperatures within the fluid itself. As well, the authors studied the pressure drop across the system to determine the overall effectiveness of the system including countenance for increased pumping powers. Ultimately, the authors state that

considering the new temperature distribution and pressure drop the use of porous foams present the opportunity for enhanced thermal performance in annular cross-flow heat exchangers.

Kurtbas and Celik (2009) performed a study into the nature of forced and mixed air convection through a porous foam filled rectangular duct. The study used three samples of 6101 aluminum foam at 10, 20, and 30 PPI. All three of the aforementioned samples were manufactured to have porosity of 0.93. After completion of the experiment several key observations were made. It was noted by the authors that the average Nusselt number increased proportionally with the linear pore density of the sample. As well, they observed that the Nusselt number increased with respect to Reynolds number until a critical Reynolds number was reached at which point the Nusselt number began to fall. Lastly, the authors argue that the improvement in thermal performance incited by the foam is a result of two factors, the fin effect of the foam, and the tripping of turbulent flow induced by the foam.

Mancin and Rossetto (2012) presented an analytical and experimental assessment on the use of forced convection in metal foams [35]. The objective of the authors herein was the extension of the already existing database of heat transfer knowledge, regarding metal foams, to include forced convection. The study used a total of twenty-one experimental samples with linear pore density ranging from 5 PPI to 40 PPI. As well the authors observed the varied porosity of the aforementioned samples. Lastly, it is worth noting that the experimenters used air as the working fluid for the experiment. Notably, the authors observed that as the linear pore density increased, the thermal performance of the system decreased. This is converse to what occurred when considering the pressure drop, where, it was observed that as the linear pore density increased the pressure drop also increased.

Yang et. al. (2014) presented an analytical model for the effective thermal conductivity of porous foam metals based on a unit cell approach [36]. The model focussed on high porosity foams, $\epsilon \geq 0.91$. The basis for the model was the use of a tetrakaidekahedral unit cell with cubic nodes. The results obtained herein were then compared to experimental data collected from the surrounding literature. The results for the effective thermal conductivity of the sample foams are presented using a very simple equation of the form:

$$\frac{k_e}{k_s} = 0.36(1 - \epsilon) \quad (3)$$

In the above expression the coefficient presented by the authors represents the *reciprocal thermal coefficient of tortuosity*. The authors further state that this coefficient functionally represents the elongated heat transfer length within a cell. Lastly, the authors observe that the effects of pore size and ligament geometry both seem to have little impact on the effective thermal conductivity of the foam fluid system.

Dukhan et. al. (2013) presented a comparison between the Brinkman-Darcy flow model and collected experimental results [37]. The experiment used forced air convection through a porously filled cylindrical tube with isoflux conditions at the walls. The authors observed good agreement between the aforementioned numerical approach and the experimental results. As can be expected it was observed that as the velocity in the system increased, so too did the pressure drop across the test section. The authors did however note that the use of the volume average energy equation, in combination with other constituent equations, did tend to under estimate the temperature throughout the entire distribution. Regardless, the authors still state that the use of such predictive models offers an approach for better understanding complex porously filled heat transfer systems.

Mancin et. al. (2013) collected experimental data on forced-air convection through foam metal in order to validate a numerical approach [38]. The paper experimentally characterized 21 samples with linear pore density ranging from 5 PPI to 40 PPI, and porosity varying between 0.896 and 0.956. As well, the authors varied the height of these porous samples between 20 mm and 40 mm. The control parameters used for the aforementioned study were air flow rate and wall heat flux. The authors observed that when comparing the two materials, the copper foam exhibited higher heat transfer performance than that of the aluminum. As well, it was observed that although the 20 mm samples offer half the heat transfer area of the 40 mm samples, they still offered improved efficiency. The authors believe this to likely be as a result of large role played by the foam finned surface efficiency parameter.

Dukhan et. al. (2015) studied experimentally thermal development in porous media under constant heat flux conditions [39]. The experiment used cooled water flow through a cylindrical tube under

constant wall heat flux conditions. The study looked at the Darcy, transitional, and Forchheimer flow regimes. The foam sample used for this experiment was made of 6101-T6 aluminum with a linear pore density of 20 PPI, and a porosity of 87.6%, manufactured by ERG aerospace. Despite over-prediction by the employed analytical model the experimenters were able to create a comparison with experimental results which allowed them to identify a very distinct thermal entry region. As well, the over-prediction which resulted from the use of the local thermal equilibrium model demonstrated distinctly that whenever possible it is more accurate to use a local thermal non-equilibrium model. The use of this model is of course limited based on computational abilities.

Fleming et. al. (2015) studied the performance of foam metal enhanced thermal storage systems using phase change materials [40]. The experiment employed the use of a shell and tube thermal storage device using water as the phase change material with the addition of foam metal. The experiment employed a metal foam with a linear pore density of 40 PPI manufactured by ERG aerospace with the objective of enhancing the heat transfer rate to the base fluid. To fit into the shell and tube storage device the foam metal was cut into disks and laid in layers. Cold water was then supplied to the outer tubes with the heated water leaving through the more central tubes. The authors observed that the use of metal foams greatly enhanced the heat transfer when employed. Notably the authors observed that for melting the enhancement was on the order of 100%, while for cooling the enhancement was to the order of 20%. The authors suggest that this deviation occurs as a result of the difference in thermal conductivity of solid and liquid water. This further suggests that the thermal conductivity of the working fluid plays a large role in the overall effectiveness of the system employing the foam metal. Further, it is worth noting that the authors observed deviation between their determined effective thermal conductivities and those stated by previous researchers.

Bagci et. al. (2015) extended their previous work to include experimental evaluation of the thermal exit effects within porous media [41]. The experimental apparatus used in the collection of this data was highly similar to that of the original, including the use of a 6101-T6 aluminum foam sample with linear pore density and porosity of 20 PPI and 87.6% respectively. The results from this experiment were then validated against an analytical approach within the Darcy regime. Again, the authors successfully demonstrated that the consideration of exit effects in porous media heat

transfer are significant. It was observed in both consideration of the Nusselt number and temperature distribution.

Chen et. al. (2018) conducted a numerical study into natural convection within a partially porous media filled square cavity with an open-end [42]. The hopes of the authors are that the results contained herein can be used in validation of future experimentation, and the development of more detailed numerical models. The authors suggest that the model developed in the work has applications in environmental engineering, particularly to be used in determining the critical thickness of porous media to be used when enhancing the performance of solar energy systems. Consistent with the authors plan they were able to successfully demonstrate that in such a cavity there existed a critical ratio between the thickness of the foam and the height of the cavity.

1.2.2 Nanofluids

The complex nature of the thermal mechanisms which drive the enhancement in thermal performance of Nanofluids is of recent interest in their use as heat transfer augmenters. Nanofluids prove to be so favourable as a result of their ability to perform well with low volume percentage concentrations. This allows them to be economically viable. The use of Nanofluids was originally limited to use in smaller heat transfer systems as a result of cost. However, now that more understanding on their behaviour has been developed, the use of Nanofluids in heat transfer systems is beginning to be seen as a feasible option for use in macroscale designs. One of the most widely argued driving forces behind the dramatic augmentation is the large surface area to volume ratio which the Nanofluids boast. In some cases, the surface area to volume ratio of a single nanoparticle can be 10000:1. This offers a massive amount of potential for use in heat transfer systems. As well, at low concentrations Nanofluids do not typically cause a significant increase in the viscosity of their base carrying fluid.

1.2.2.1 Numerical Modeling

Similarly, to the study of fluid flow involving Nanofluids the computational limitations of current simulation systems has widely been the controlling factor in the development of models for heat transfer in Nanofluids. The thermal transport phenomena which surround Nanofluids are complex and depend on a large number of factors, including, particle geometry, temperature gradients, ratio of internal driving forces, direction of flows relative to gravity, and so on. As such, there has been

a large effort made to characterize Nanofluids as homogeneous fluids utilizing characteristics similar to those of more conventional fluids. Once again, this is achieved using various modifying parameters and statistical relationships.

Xu et. al. (2015) studied numerically the flow and heat transfer characteristics of Nanofluids interacting with porous media [43]. The study used a rectangular porously filled duct for the flow simulation. Notably, the authors observed that with increasing Nanofluid concentration both the pressure drop and Nusselt number distribution increased. However, they did notice that after a certain critical concentration, the rate at which the pressure drop increased continued to grow, while the rate at which the Nusselt number increased lowered. This then implies that for a given Nanofluid system there will exist a critical concentration at which the ratio between pressure drop and thermal augmentation is a maximum. After said critical point the increase in required pumping power will outweigh the gain in thermal augmentation, and as such, it is more viable to pursue other methods of thermal performance enhancement. As well, they observed that the velocity profile of a Nanofluid through the foam metal is very linear, while the thermal non-equilibrium is more obvious, particularly when the difference between the thermal conductivity of the fluid and the particle are large. Lastly, the authors note that the use of field synergy principle for conventional fluid systems cannot be used to accurately predict the behaviour of Nanofluids.

Ameri et. al. (2017) conducted a study on the thermal performance of Nanofluids in a metal foam filled tube, with consideration of heterogeneous Nanoparticle distribution [44]. The heterogeneous model herein referred to as the *thermal dispersion approach*, was shown to improve the accuracy of predictions based on experimental data when compared to the more classical homogeneous approach. Particularly, the authors note that the conventional approach seemed to consistently underestimate the systems behaviour. A similar trend was observed when the velocity distribution was considered. Lastly, the authors observed that the Nusselt number increased with increasing Nanoparticle concentration and decreased as the porosity increased for a given Reynolds number.

Karimi and Afrand (2018) conducted a numerical study into the thermal performance of hybrid Nanofluids in pipe arrangement and cross-sections [45]. The Nanofluid used for the simulation was a hybrid Nanofluid designated MgO-MWCNTs/EG. This Nanofluid is required to act as the working fluid within the aforementioned radiator system. Significantly, the authors noted that the vertically oriented radiator system performed 10% more efficiently than its horizontally oriented

counterpart. Further the authors observed that the increasing concentration of the Nanofluid concentration was the primary driving factor for the improvement of the Nusselt number. Specifically, noting that an increase of 1% in Nanofluid concentration lead to a 50% increase in Nusselt number. However, a similar yet staunchly steeper trend was observed with the pressure drop, wherein even a slight increase in Nanofluid concentration resulted in a stark increase in the pressure drop through the system. This staunch increase in pressure drop was believed to be a result of the increase in the fluid viscosity.

1.2.2.2 Experimental Study

As was observed in the experimental study of Nanofluids with an emphasis on fluid flow behaviour, the experimental study of thermal transport phenomena involving Nanofluids is also limited as a function of cost. However, when considering heat transfer and thermal augmentation involving Nanofluids there is considerably more work being done. This is likely as a result of the substantial augmentation at low volume concentrations. This is notably converse to what is typically observed when considering fluid flow and Nanofluids, wherein the use of Nanofluids typically proves unfavourable for flow augmentation.

Nazari et. al. (2015) studied the effects of Nanofluids under forced convection conditions through a pipe filled with metal foam [46]. The study employed the use of an Al_2O_3 -water Nanofluid passing through an aluminum porous medium with porosity of 50%. The Nanofluid concentration was varied from 0.1% to 1.5%. It was observed that the Nusselt number increased at constant Reynolds number with increasing Nanofluid concentration, with water being the lowest. Further, it was observed that for all concentrations of Nanofluid the addition of porous media increased the Nusselt number as well. However, it was noticed that the combination of higher concentration Nanofluid with porous media did result in a significant increase in the pressure drop across the system. This pressure drop was to the order of 50%. Over all the authors do believe that such combined heat transfer systems prove to be viable candidates for heat transfer applications.

Jouybari et. al. (2017) studied experimentally the effects of both porous media and Nanofluid on the performance of flat-plate solar collectors [47]. The study considered the use of SiO_2 -deionized water Nanofluid at concentrations of 0.2%, 0.4%, and 0.6%. The authors observe that when considering the efficiency of the solar panel, increasing the Nanofluid concentration has a greater

effect than increasing the flow rate. Moreover the authors note that as the efficiency of the solar collector is in part a function of the pressure drop across the test section, there does exist a critical Nanofluid concentration. At said concentration, the pressure drop due to the increased fluid viscosity outweighs the benefit seen by the increased thermal conductivity and increasing the Nanofluid concentration becomes inviable for a practical system.

Buschmann et. al. (2018) presented a collection of 5 different forced convection experiments with the objective of establishing a more realistic set of guidelines which can be employed when working with Nanofluids [48]. While the article did present five complete experiments including results, the primary focus of the paper was the outlining of the following rules. The first of these rules stated that the employment of single-phase Newtonian fluid flow was sufficient when considering the Nusselt number and other such dimensionless factors. The second rule states that under similar fluid flow conditions, Reynolds number, Prandtl number, etc.; the driving mechanism in thermal performance augmentation lies in the difference in thermal conductivities between the constituent fluid and the Nanoparticles. The third and final statement simply notes the above two statements held true across several widely diverse industrial test systems. The combination of these three realities allows for the use of a dramatically simpler method of analysis when considering Nanofluids. Similar, to previous work completed to date the authors present the conventional heat transfer equations with modifying coefficients based on the concentration of Nanoparticles relative to the base fluid.

Akshay et. al. (2018) studied experimentally the enhancement of thermal performance of a loop heat exchanger with the addition of alumina-water Nanofluid [49]. The study considered deionized water for a baseline case against 2% mass concentration alumina-water Nanofluid. It can be observed based on the presented data that at a given applied power the temperature of the system using Nanofluid fell lower than that of the water baseline. Specifically, the author stated that a 12% decrease in this temperature was observed. Additionally, the authors observed that the system employing Nanofluid was more readily able to reach steady-state operating conditions. The authors conclude that the combination of these two factors can be used to demonstrate alumina Nanofluids as feasible heat transfer enhancers in loop heat exchangers.

Bayomy et. al. (2016-2017) studied the performance of both Nanofluids and foam metals as heat exchange enhancers [50] [51] [52]. The studies thoroughly analyzed the effects of Nanofluid

concentration, channels, and foam metals on the thermal performance of heat exchange systems with applications in electronics cooling. Among the objectives of the current study is the goal to expand the knowledge initially established by the authors and to extend the study to fill in potential voids of information. Particularly, where the relationship between concentration and channels is concerned. The authors established an index of thermal performance which considered the thermal and pressure effects on the system.

Saghir, Welsford, et. al. (2018-2019) studied the effects which both Nanofluids and highly porous foam metals have on the performance of various thermal systems including applications in electronics and thermal storage [53] [54]. The authors employed a similar computational and experimental approach to that in the present study. It was observed that as the permeability increased under constant flow rate the thermal enhancement also improved. As well, the authors observed good agreement between the experimental and numerical results. Lastly, it was observed that when Nanofluid was added to the system the thermal performance was improved.

2 Experimental Procedure and Apparatus

To verify computational work, empirical data with which the results can be compared is necessary. The experimental apparatus which is used in the present study is based on that which was originally developed by Bayomy et. al. [50]- [52]. The system is designed in such a way as to replicate an intel i7 processor. The geometry of the heater is set to match that of the chipsets integrated heat spreader. The heat flux which passes through the simulated heater is set to match the losses which an actual CPU would experience under an extremely demanding computational load.

2.1 Apparatus and Procedure

The experimental apparatus in the present study consisted of six main components. The first component is a set of three pumps. The pumps are plumbed in parallel to ensure that the system has sufficient pressure to push the working fluid through the entirety of the system. Multiple pumps were selected to ensure stable and fluid flow. A single large pump posed the potential to introduce inherent pulsation to the fluid. Following the pumps was a flow control valve. The valve allowed the manipulation of the flow rate through the system. This is necessary as it allows the flow rate to be set within the laminar regime and to be varied between studies. The third component was an inline flow meter. The flow meter allows the recording of the real flow rate through the system. After a steady flow was established the fluid passed through the experimental test section shown in Figure 1. The test section was designed to be opened to allow the test sample to be changed. The samples used in the present work are both made of 6061-T6 open cell foam metal. The metal foam is guaranteed by the manufacturer, ERG Aerospace, to be homogeneous in nature [55]. The samples both had a porosity of 91% and a linear pore density of 40 pores per inch (PPI). Further, the experimental test section is equipped with ten T-type thermocouples which are used to collect the surface temperature distribution and the inlet and outlet temperature. The cross-section of the test area is shown in Figure 2. Once the fluid passes through the test section it is pushed through a helical heat exchanger which is connected to a constant temperature water bath. This is done to stabilize the inlet temperature of the system. Inlet temperature stability is important for reproducibility, and to allow the system to reach steady state within a reasonable period. Lastly, after passing thorough the heat exchanger the fluid is returned to a fluid reservoir where it then returns to the pumps. The apparatus is shown schematically in Figure 3.

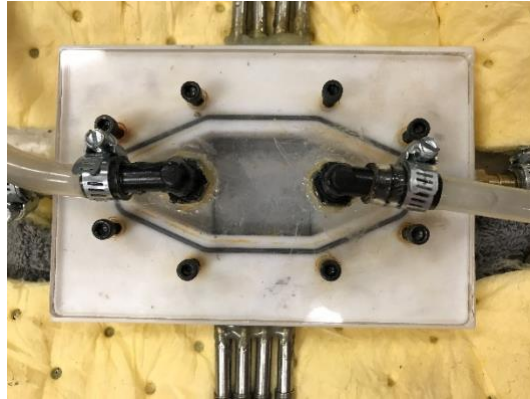


Figure 1: Experimental Test Section

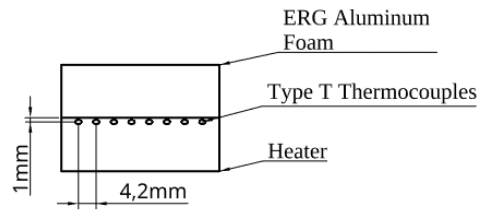


Figure 2: Cross-Section of Test Area

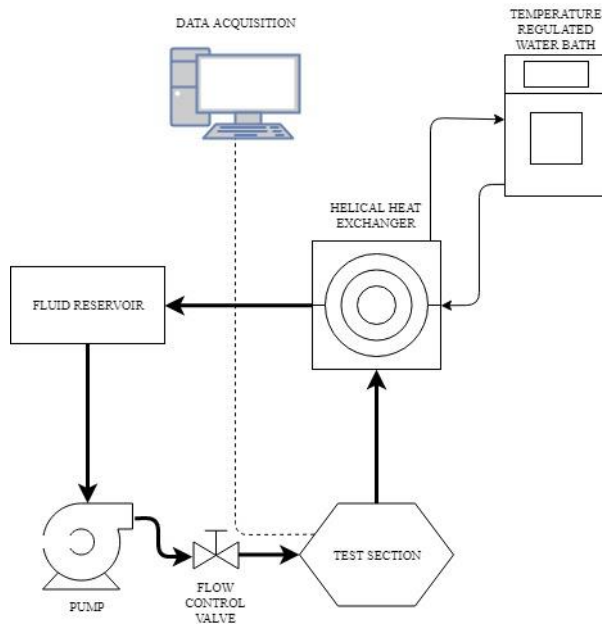


Figure 3: Schematic of Apparatus

The working fluid used in the present study was γ -Al₂O₃-water Nanofluid prepared by MK Nano [56]. The fluid is guaranteed to be in a stable mono-dispersed mixture. Further, the solution is designed in such a way as to prevent the agglomeration of the Nanoparticles. The stock solution was supplied at 20% by volume and was diluted to the required concentration. The concentrations used in present are 0.1%, 0.3%, and 0.6% by volume. The concentration was intentionally kept low as the cost of the Nanofluid is high. Reducing the concentration then increases the commercial viability of any design solution into which the mixture may be added. Lower concentrations are more economically viable.

The solutions were prepared through dilution of the supplied stock solution. To dilute the solution the concentration of the solution was converted from volume fraction to mass fraction. This conversion allowed the researchers to use a highly sensitive scale to measure the mass of each component inserted into the mixture.

The batches were then mixed in 50-gram independent batches which were transferred to a larger container. This was done to allow the use of a higher resolution scale when weighing the samples.

Once 500-grams of solution was prepared the container containing the mixture was put on a magnetic stirring plate to ensure that the solution was uniformly dispersed. The solution was allowed to mix for 20 minutes per batch.

Once the solution was mixed it was transferred to a larger container to be used for filling the system.

The placement of the test samples into the test section is crucial when considering experimental repeatability. This sensitivity to sample placement is a result of the thermal contact resistance which exists between the sample and the simulated heater. To minimize the thermal contact resistance, thermal compound is applied to the surface of the heater before the sample is inserted. It is important that the thermal compound is spread evenly and to the same thickness between each study. Deviations in the thickness of the thermal paste can result in poor thermal contact which skews the inward heat flux. To help reduce the effects of thermal contact resistance the same sample was used for as many consecutive tests as possible before changing. This means that the sample should only be changed after all flow rates and heat fluxes have been tested. Further, if care is taken when removing the sample from the test section the existing thermal paste can

typically be used for the subsequent sample. This implies that the thermal compound should only be removed after completing a test for an entire concentration.

The sample was then inserted into the test area and the solution was added to the system. When adding the solution to the closed system great care must be taken to not splash surrounding electronics or any other equipment. Further, it is of great importance that care is taken to avoid contamination of the samples and the system during the fluid addition.

The isothermal water bath was turned on to start cooling to a temperature of 4 °C. The flow from the water bath across the helical heat exchanger was set to a point that all coils were submerged. It is important that the fluid be allowed to circulate over the operating heat exchanger before the water within the bath reaches temperature. If the bath is allowed to reach operating temperature before the water is circulated a spike is observed in the bath temperature and more time must be given as the system reproaches the set point.

The pumps were then turned on to begin the circulation of the fluid and the inline valve was used to set the system flow rate for the system.

The heater was then set to a current of either 1.0, 1.2, or 1.4 Amperes. Care should be taken to monitor the inbound current as deviations from the required nominal values can propagate through subsequent analysis and cause large deviation between numerical and experimental results.

The system was then allowed to continually operate while the temperature distribution of the heater surface was monitored. Once the surface temperature stabilized the system was deemed to be operating under steady-state conditions. The system temperature was considered stable when the change in measured temperature was less than 0.1 °C per 5-minute interval.

At this point the measured temperatures, heater voltage, heater current, and flow rate were recorded.

After the completion of a set of tests the test sample was removed, and the system was drained completely and flushed with distilled water. This was done to prevent the build-up of contaminants within the system. Several days were left between tests to allow the residual water to evaporate out of the system. After each test the samples used were thoroughly rinsed with distilled water to ensure that no contaminants had been trapped within the porous cells. As well, the thermal paste

was washed off the bottom of the porously filled channel sample as the thermal paste tended to stick to the flat bottom surface of the sample.

2.2 Uncertainty and Error Analysis

When considering any experimental study, the analysis of the inherent system uncertainty is crucial to understanding how the system behaves. The primary experimental measurement in the present study is temperature. The present study employed ten T-type thermocouples to measure the systems temperature. The uncertainty for the thermocouples was determined through the calibration conducted by Bayomy et. al. [50] during the original study to be 0.75% ($^{\circ}\text{C}$). Similarly, to the uncertainty within the temperature measurements, the uncertainty obtained for the flow meter used was equal to 0.44% (USGPM) based on the calibration completed by Bayomy et. al. [50]. The third major source for uncertainty within the present study is derived from the measured heat flux. The deviation in the heat flux is primarily a function of three system parameters, the input current, the input voltage, and the thickness of the thermal paste layer used in the apparatus. The current and voltage into the heater were controlled in part by the output from the wall outlet which was used to power the system. The current in the system varied by 2% based on observed deviation within the measurement. Using a similar approach, the voltage was observed to vary by approximately 1.7%.

The uncertainty is then propagated through subsequent calculations which are used to assess the performance of the system. One such of these parameters is the Nusselt number. Taking for example the Nusselt number, the uncertainty can be determined using the Taylor method as shown in equation (4).

$$\delta Nu_x = \sqrt{\left(\frac{\partial Nu_x}{\partial x} \cdot \delta x\right)^2 + \dots + \left(\frac{\partial Nu_x}{\partial y} \cdot \delta y\right)^2 + \dots + \left(\frac{\partial Nu_x}{\partial z} \cdot \delta z\right)^2} \quad (4)$$

Where x, y, and z represent the variables within the Nusselt number including temperature and fluid velocity. As such, the error values obtained therein can then be used to develop error bars for dimensionless distributions. The maximum temperature uncertainty observed was 0.83 $^{\circ}\text{C}$ corresponding to a temperature measurement of 110 $^{\circ}\text{C}$. The maximum uncertainty observed for the Nusselt number was 1.8% corresponding to a measured Nusselt number of 96.32.

3 Finite Element Formulations and Boundary Conditions

When considering the use of commercial software for the evaluation of engineering systems, the application of appropriate system conditions, combined with an understanding of the software's operation, is necessary to produce meaningful results. The selection of the system conditions for this study was done through comparison with the experimental setup used in this paper. This was done to test the software's ability to match numerical results with real-world testing and as such empirically validate the model. The governing equations and meshing conditions were set and controlled automatically by the commercial software in the COMSOL® Multiphysics engine [57]. These conditions and equations are outlined in the following section.

3.1 Governing Equations

The selection of terms used in the governing equations of a numerical system is crucial to ensure that the results accurately represent the experimental system while efficiently using computational power. The parameters and their respective units used within the present study are velocity denoted by u in m/s, temperature denoted by T in °C, the pressure denoted by p in the units of Pascals, and power terms denoted by Q with the units of Watts. The following assumptions are made in the development of the internal governing equations. The fluid within the system is incompressible, the incompressibility of the system is represented by equation (5).

$$\rho \nabla \cdot \mathbf{u} = 0 \tag{5}$$

The system is operating at steady state. This assumption is made on the basis that the associated experiment is allowed sufficient time to reach an equilibrium state. Further, the solid-fluid interfaces are assumed to be operating at local thermal equilibrium. This assumption is made again on the premise that the system is being allowed sufficient time to reach an equilibrium state. It is assumed that the porous regimes of the study are fully fluid saturated. This assumption was made based on the experimental conditions which existed and are associated with the numerical study. Lastly, it is assumed that the working fluid can be modeled as a single-phase fluid. This assumption is made based on the work by Ho et. al. [8] - [11]. The fluid properties used in the present study are shown in Table 1 below and are based on the work by Ho et. al. [8] - [11].

Table 1: Nanofluid Properties Obtained from Ho et. al. (2008-2013)

Concentration by Volume (%)	μ_{nf} $\left(\frac{kg}{m \cdot s}\right)$	ρ_{nf} $\left(\frac{kg}{m^3}\right)$	$C_{p_{nf}}$ $\left(\frac{J}{kg \cdot K}\right)$	k_{nf} $\left(\frac{W}{m \cdot K}\right)$
0.1	0.001007	1000.802	4169.708655	0.614817
0.3	0.001019	1006.005	4145.316698	0.618523
0.6	0.00104	1013.811	4109.19825	0.624262

In order to implement these fluid properties within the current simulation a custom domain material was defined. There exist several key equations which govern the movement of thermal energy and fluid within the system. The first of these is the continuity equation for the free fluid flow defined inequation (6).

$$\rho \nabla \cdot \mathbf{u} = 0 \quad (6)$$

The continuity equation for the fluid within the porous media is defined as shown in equation (7).

$$\rho \nabla \cdot \mathbf{u} = Q_m \quad (7)$$

Once continuity is established for the fluid throughout the complete system it becomes necessary to establish momentum conservation for the system. For the free domain the system momentum is defined using the general Navier-Stokes equation as shown in equation (8).

$$\rho(\mathbf{u} \cdot \nabla)\mathbf{u} = \nabla \cdot [-p\mathbf{I} + \mu(\nabla\mathbf{u} + (\nabla\mathbf{u})^T)] + \mathbf{F} \quad (8)$$

The conservation of momentum within the porous domain is governed according to the Darcy-Brinkman-Forchheimer equation. This equation includes considerations for viscous effects of the fluid. The expression is shown in equation (9).

$$\frac{\rho}{\epsilon_p} \left((\mathbf{u} \cdot \nabla) \frac{\mathbf{u}}{\epsilon_p} \right) = \nabla \cdot [-p\mathbf{I} + \frac{\mu}{\epsilon_p} (\nabla \mathbf{u} + (\nabla \mathbf{u})^T)] - \left(\mu k^{-1} + \beta_F |\mathbf{u}| + \frac{Q_m}{\epsilon_p^2} \right) \mathbf{u} + \mathbf{F} \quad (9)$$

Having established the behavior of the fluid within the system it now becomes necessary to establish the equations which govern the movement of thermal energy through the system. In the free fluid domains, the general convective heat transfer equation was adopted. This equation is shown in equation (10).

$$\rho c_p \mathbf{u} \cdot \nabla T_2 + \nabla \cdot \mathbf{q} = Q + Q_p + Q_{vd}, \text{ where } \mathbf{q} = -K \nabla T_2 \quad (10)$$

The heat transfer equation used in the porous domain of the present study is defined similarly to that of the general heat transfer equation. However, there exists a variation within the definition of \mathbf{q} wherein K is substituted with K_{eff} . K_{eff} is defined in equation (11).

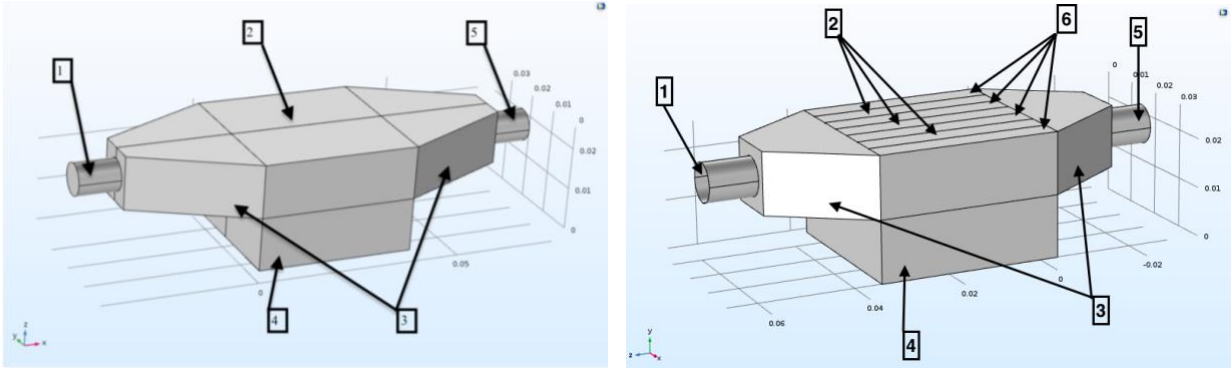
$$k_{eff} = \theta_p k_p + (1 - \theta_p)k + k_{disp} \quad (11)$$

To improve the accuracy of the modeled effective thermal conductivity the values used for the solid fraction of the porous media were substituted using the model developed by Boomsma et. al. [21]. The thermal conduction through the solid system domains is defined in equation (12).

$$\rho c_p \mathbf{u} \nabla T_2 + \nabla \cdot \mathbf{q} = Q = Q_{ted}, \text{ where } \mathbf{q} = -k \nabla T_2 \quad (12)$$

3.2 Boundary Conditions and Domains

The boundary conditions which were applied to the numerical system, were as previously mentioned, selected in a manner which would most realistically represent the physical experiment which took place. The following study necessitated the creation of two Multiphysics models as a result of the geometric differences incited by the introduction of porous channels. The domains and boundary conditions for the purely porous and porous channel models are shown in Figure 4 (a) and (b) respectively.



(a)

(b)

Figure 4: Domains and Boundary Conditions for (a) Purely Porous Model and (b) Porous Channel Model

The domain condition which corresponds to each value shown in Figure 4 is shown in Table 2 below.

Table 2: Numerical System Domains

Caption Number	Bulk Media	Channel Media
1	Purely Fluid Inlet	Purely Fluid Inlet
2	6061-T6 Aluminum foam metal	6061-T6 Aluminum Foam Metal
3	Purely Fluid Domain	Purely Fluid Domain
4	Solid 6061-T6 Aluminum	Solid 6061-T6 Aluminum
5	Purely Fluid Outlet	Purely Fluid Outlet

6	N/A	Solid 6061-T6 Aluminum
---	-----	------------------------

For both of the above described systems the boundary conditions can be defined as follows. The inlet for both systems was set as a fixed fluid velocity with a constant temperature. The fluid velocity was determined using the cross-sectional area of the inlet and the flow rate. The inlet temperature was determined based on experimental results. The outlet of the system was set to be free and open for both fluid and thermal energy. This was done to maintain conservation of energy within the system. The boundary between the foam metal and the solid aluminum was modeled using a thin layer to replicate thermal contact resistance. A constant inward heat flux was applied to the bottom of the solid aluminum block which mimicked the measured power from the heater used in the experiment. Lastly, all other surfaces of the system were modeled as non-slip, thermally insulated walls. The definitions for the boundary conditions are shown in equation (13) through (20) below.

$$\mathbf{u} = u_0 \quad (13)$$

$$T = T_0 \quad (14)$$

$$[-pI + \mu(\nabla\mathbf{u} + (\nabla\mathbf{u})^T)]\mathbf{n} = -\hat{p}_0\mathbf{n}, \text{ where } \hat{p}_0 \leq p_0 \quad (15)$$

$$-\mathbf{n} \cdot \mathbf{q} = 0 \quad (16)$$

$$R_s = \frac{d_s}{k_s} \quad (17)$$

$$-\mathbf{n} \cdot \mathbf{q} = q_0 \quad (18)$$

$$u = 0 \quad (19)$$

$$-\mathbf{n} \cdot \mathbf{q} = 0 \quad (20)$$

The initial conditions of the fluid and solid domains within the system are defined based on the measurement of the atmospheric conditions within the experimental environment at the time the study was conducted. These above conditions and equations define the physics of the system at all of its boundaries.

3.3 Meshing and Finite Element Scheme

The development of a finite element mesh for the analysis of the system was done automatically using the integrated physics controlled meshing system. The details of the meshing scheme employed in the present study are shown in Table 3.

Table 3: Finite Element Meshing Scheme

Element Type	System Type	
	Bulk Porous Media	Porously Filled Channels
Domain Elements	648834	1441256
Boundary Elements	44554	83351
Edge Elements	1609	2701

The mesh employed in the finite element study corresponded to the *finer* setting in COMSOL. This mesh was determined to be appropriate as it balanced computational demand with system stability. A mesh sensitivity study was conducted to ensure that the system was stable. The results of this study are shown in Figure 5.

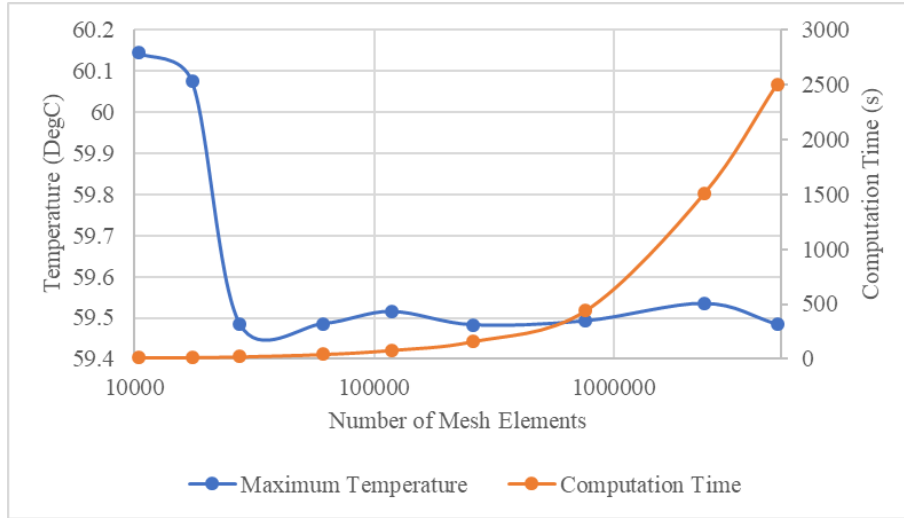


Figure 5: Mesh Sensitivity Study

The mesh sensitivity study shows a clear over-estimation, indicated in Figure 5, of the maximum system temperature until the simulation reaches approximately 27000 mesh elements. At this point the temperature begins to stabilize. The finer mesh setting corresponds roughly to 750000 mesh elements. It can be seen at this point that the computational time required per study intersects the maximum temperature curve. As well the deviation in study time between the fine and finer mesh only increases slightly. Whereas, the change in computational time for finer to extra fine increases significantly. The final meshing schemes selected for both the 3 channel and bulk porous heat sink are shown in Figure 6.

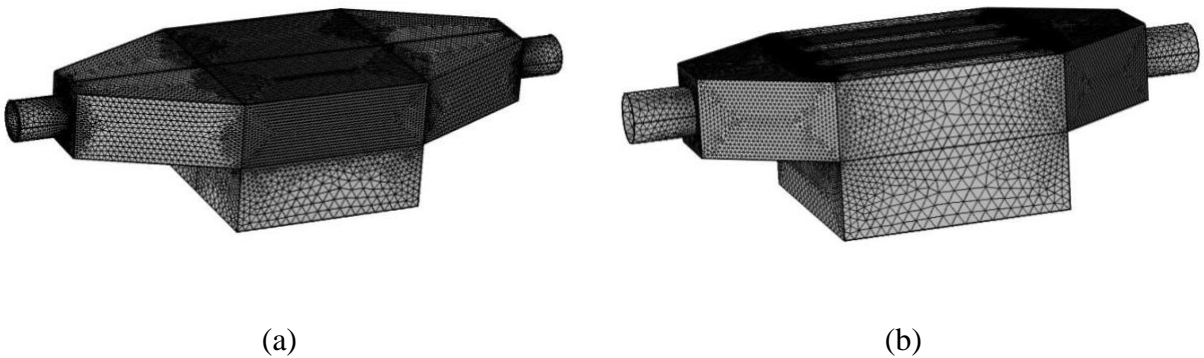


Figure 6: Meshing Scheme for (a) Bulk Media and (b) Porously Filled Channels

4 Discussion and Analysis of Results

To determine the impact which the various experimental parameters had on the system performance three key system properties were used. The first was the surface temperature distribution of the heater. This represented the raw data which was recorded. The second was the dimensionless Nusselt number. This term was used to show the strength of the convective mechanism within the studied system configuration. The Nusselt number is defined in equation (21).

$$Nu = \frac{hD_e}{k} \quad (21)$$

Where h is the convective heat transfer coefficient defined in equation (22).

$$h = \frac{q''}{T - T_{in}} \quad (22)$$

In the present study the average Nusselt number will be used to determine the performance of the system from a perspective of pure heat transfer. However, when considering a real fluid, it becomes important to consider the effects on power requirements which the fluid properties have on the system. In the present paper the pressure drop and an index of performance defined by Bayomy et. al. [52] will be used to determine the effectiveness of the system when considering both heat transfer and pumping power. The index of performance is defined in equation (23).

$$I_{performance} = \frac{Nu_{avg}L}{f_{friction}H} \quad (23)$$

Within this parameter $f_{friction}$ is the Fanning friction factor, L is the length of the sample, and H is the height of the sample. The Fanning friction factor is defined in equation (24).

$$f_{friction} = \frac{\Delta P}{4 \left(\frac{L}{D_e}\right) \left(\frac{\rho u^2}{2}\right)} \quad (24)$$

The four experimental parameters which were varied within the present study are: flow rate, heat flux, Nanoparticle concentration, and geometry of the test section. The study considered 3 primary flow rates of 0.1, 0.2, and 0.3 USGPM. As well, three heat fluxes were studied with nominal values of 50000, 75000, and 100000 $\frac{W}{m^2}$. Further, 3 concentrations were studied at present, 0.1% 0.3%, 0.6% by volume. Lastly, two heat sink geometries were employed, the first considered only bulk porous media, the second considered three porously filled channels.

4.1 Effect of Flow Rate on System Performance

When considering a forced convection system, it is typically expected that an increase in the flow rate will reflect an increase in the heat removal rate. The following represents the effects which flow rate has on the system while being subjected to a constant nominal heat flux of 50000 $\frac{W}{m^2}$. The flow rates used in the present study are 0.1, 0.2, and 0.3 USGPM for the 0.3% and 0.6% samples, and 0.2, 0.4, and 0.6 USGPM for the 0.1% sample. A higher flow rate was selected for the 0.1% sample as there exists a large amount of empirical data in the literature surrounding this concentration's use. The 0.2 USGPM flow rate was selected to allow comparison between all concentrations. The maximum relative error between the numerical and experimental temperature distributions which follow is 4.3%, thus showing good agreement. Figure 7 shows the temperature distributions associated with the 0.1% concentration for both the bulk and porously filled channel samples.

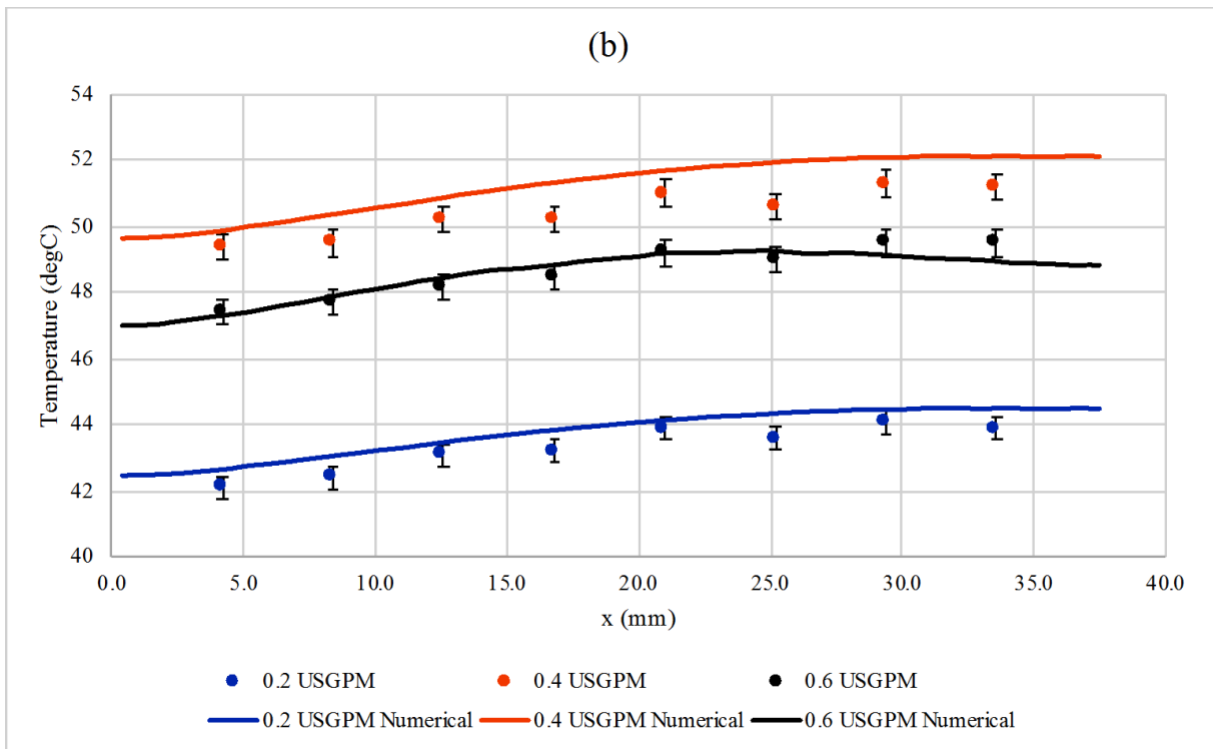
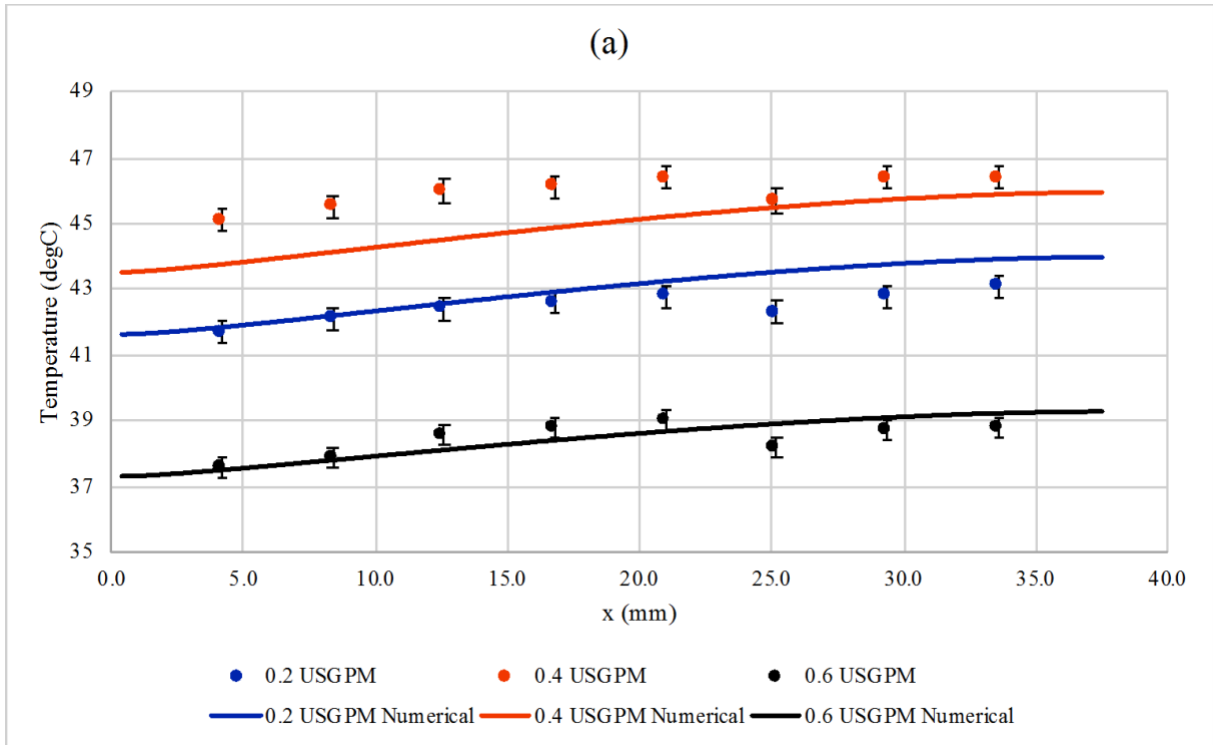


Figure 7: Temperature Distributions at Constant Heat Flux for (a) Bulk Media (b) Poursly Filled Channels

The results show an unclear relationship between the flow rate and the temperature distribution through both samples. It would be expected that the temperature distribution decrease as the flow rate increases. However, it can be seen here that between 0.2 USGPM and 0.4 USGPM there is an increase in temperature distribution followed by a subsequent drop when the flow rate is increased to 0.6 USGPM. The Reynolds number associated with the 0.2, 0.4, and 0.6 USGPM flows are 500, 1000, and 1500 respectively. It is likely that the inconsistent behaviour of the heat transfer system at these higher flow rates is connected to a transition in the flow regime. This potential for transition in flow is unfavourable when considering the use of the heat sinks in engineering applications. The pressure drops and mean velocity across the test samples are shown in Table 4.

Table 4: Numerical Pressure Drop and Mean Velocity by Flow Rate for 0.1% Nanofluid

Flow Rate (USGPM)	Bulk Media		Porously Filled Channels	
	Pressure Drop (Pa)	Mean Velocity (m/s)	Pressure Drop (Pa)	Mean Velocity (m/s)
0.2	3.845678	0.029531	14.12916	0.012377
0.4	7.273833	0.066359	29.3506	0.025818
0.6	10.27042	0.107532	39.89719	0.035435

Due to the sensitive nature of the flow within the porous system it is difficult to accurately measure the pressure and fluid velocity experimentally. To circumvent this interference the numerical model was validated using temperature values. The values for pressure and velocity were then taken from this numerical system. When considering the pressure effects, it quickly becomes clear that the inclusion of channels impacts the system performance heavily. The minimum pressure of the porously filled channel model exceeds the maximum value obtained for the bulk medium. It is likely that this is a result of the reduced cross-sectional area through which the fluid is being forced. Further, the velocity of the porously filled channels is substantially lower than that of the bulk media. This reduction in mean fluid velocity is likely a result of the effects of the increased wall surface area with which the fluid is interacting. In order to assess the viability of the both the fluids and test section geometries as heat transfer systems it becomes necessary to employ the above described evaluating criteria. The average Nusselt number and Fanning friction factor are shown in Table 5.

Table 5: Average Nusselt Number and Fanning Friction Factor for 0.1% Nanofluid at Constant Heat Flux with Varied Flow Rate

Flow Rate (USGPM)	Bulk Media		Porously Filled Channels	
	Nu_{avg}	$f_{friction}$	Nu_{avg}	$f_{friction}$
0.2	54.2658	1.116248	58.4218	23.34693
0.4	28.2604	0.418127	24.8026	11.14592
0.6	36.7112	0.224831	25.8380	8.043066

Combining all previously stated values it becomes possible to use the index of performance to establish an optimal system as a function of both the thermal performance and required pumping power. The index of performance is shown as a function of flow rate for both geometries in Figure 8.

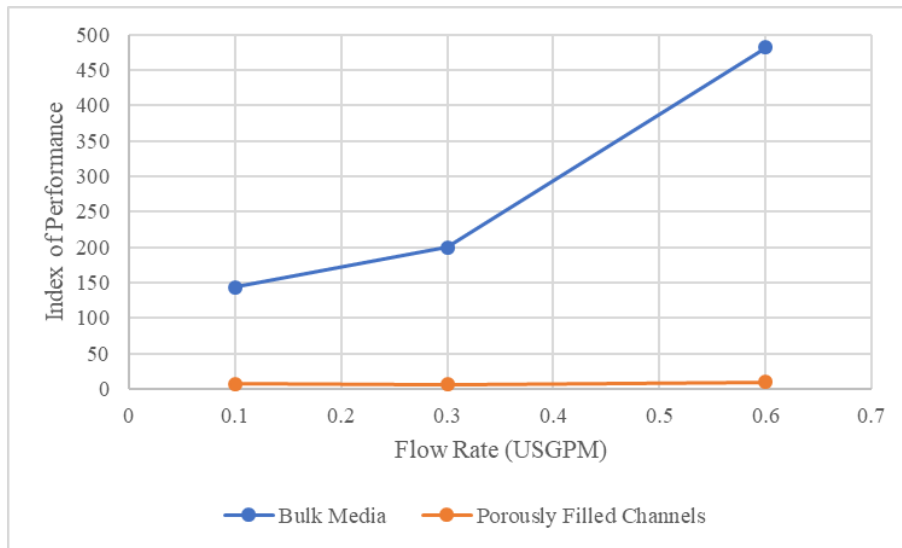
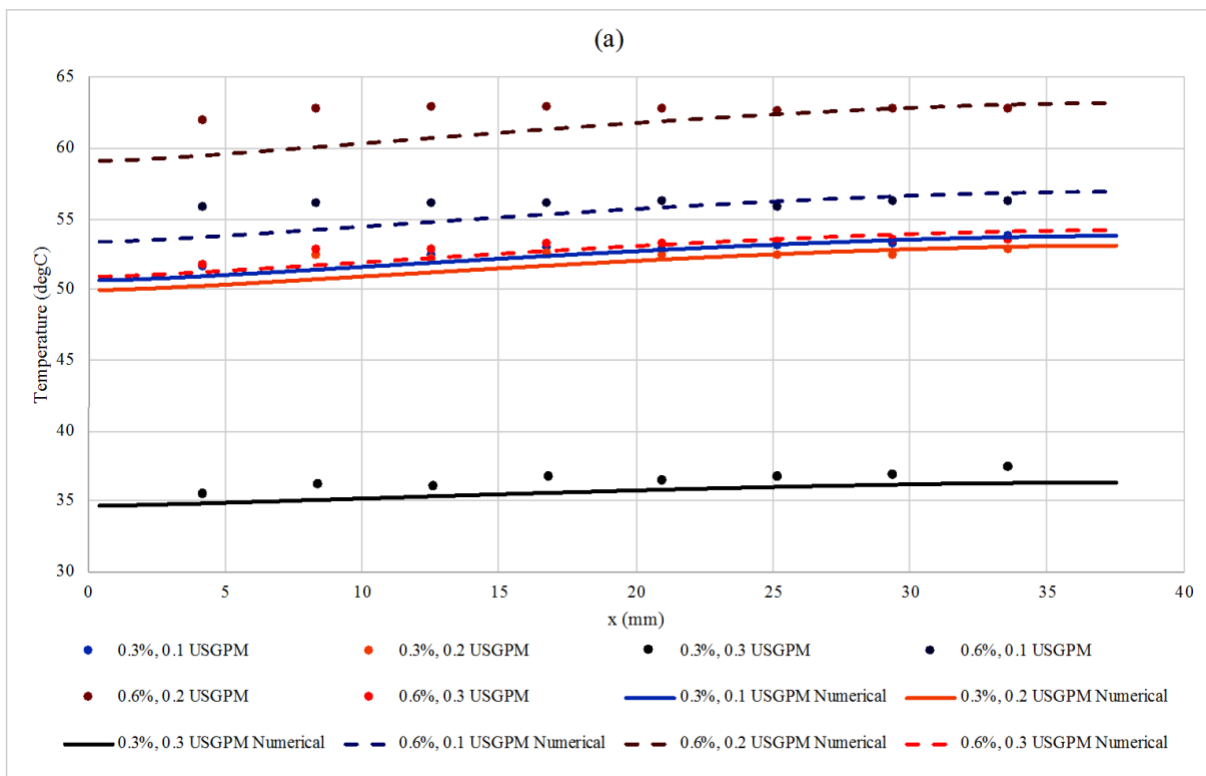


Figure 8: Index of Performance for Bulk and Channel Geometries

It immediately becomes clear that the influence of the increased system pressure plays a large role in the viability of the system. The increased resistance to the flow from the wall fluid interactions greatly reduces the velocity of the fluid through the system and as such increases the Fanning friction factor by approximately one order of magnitude. Further, the lower fluid velocity greatly reduces the order of the average Nusselt number. Combining these factors yields a dramatically

lower value for the performance index when the channels are employed. However, it can be noted that both trends share a common growth in the thermal performance as the flow rate is increased.

The remaining concentrations of 0.3% and 0.6% by volume were both studied at flow rates of 0.1, 0.2 and 0.3 USGPM. These lower flow rates were selected to allow comparison to future research as lower flow rates tend to be more popular. This will then allow other researchers to use the data from the present study for advancement of the field. The temperature distributions for the 0.1% and 0.3% concentrations interacting with both the bulk and channel geometries are shown in Figure 9.



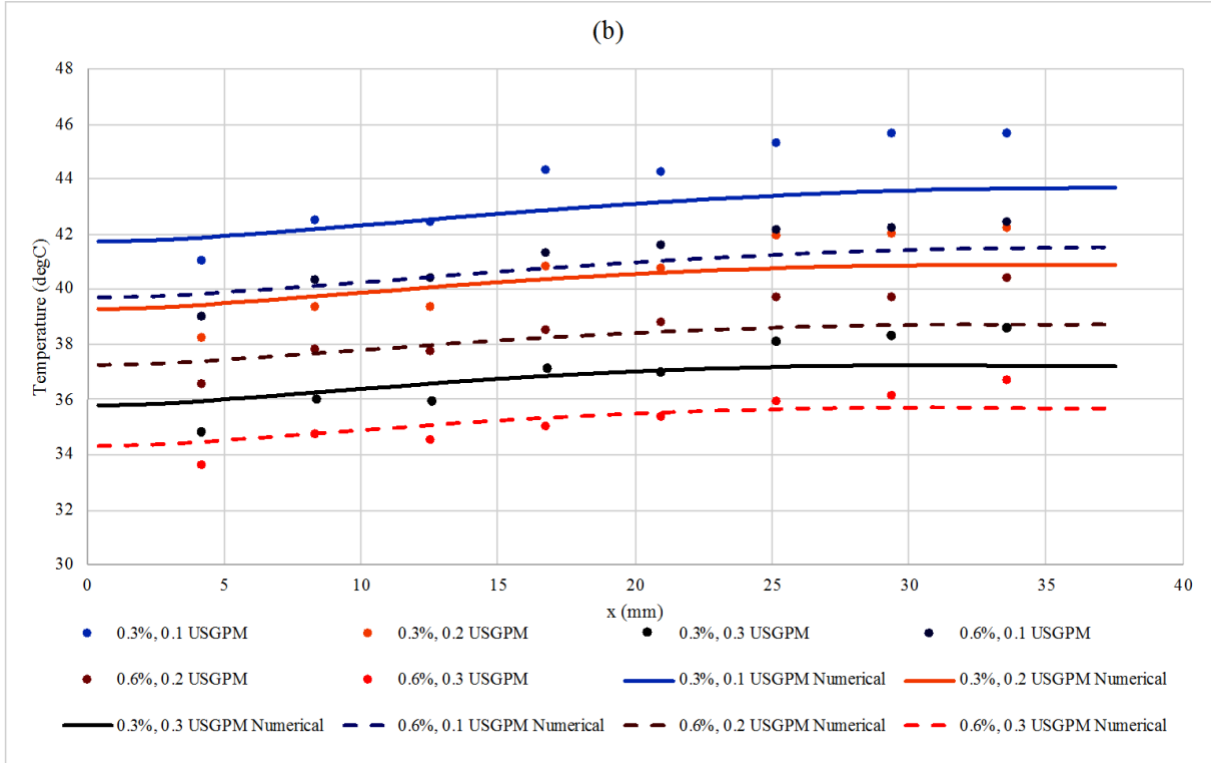


Figure 9: Temperature Distributions for 0.3% and 0.6% interacting with (a) Bulk Media and (b) Porously Filled Channels

In Figure 9 (a) it can be seen that as the flow rate increases the temperature distribution decreases. This consistency with expectations which was not observed at the higher flow rates likely occurred as the Reynolds number corresponding to the three flow rates are 300, 570, and 800 for 0.1, 0.2, and 0.3 USGPM respectively. This lower Reynolds number is more consistent with a perfectly laminar flow. This then shows that when considering the flow rate for engineering applications it is favourable to increase the value as high as is possible without entering the transitional regime. Similarly, to the higher flow rates it is important to characterize the pumping requirements for both remaining concentrations. The numerically obtained pressure drops and velocity are shown in Table 6 and Table 7.

Table 6: Numerical Pressure Drop and Mean Velocity by Flow Rate for 0.3% Nanofluid

Flow Rate (USGPM)	Bulk Media		Porously Filled Channels	
	Pressure Drop (Pa)	Mean Velocity (m/s)	Pressure Drop (Pa)	Mean Velocity (m/s)
0.1	1.983820	0.014136	6.973488	0.006062
0.2	3.876564	0.029539	14.293294	0.012374
0.3	5.687503	0.047083	21.879553	0.018950

Table 7: Numerical Pressure Drop and Mean Velocity by Flow Rate for 0.6% Nanofluid

Flow Rate (USGPM)	Bulk Media		Porously Filled Channels	
	Pressure Drop (Pa)	Mean Velocity (m/s)	Pressure Drop (Pa)	Mean Velocity (m/s)
0.1	2.025171	0.014133	7.114791	0.006058
0.2	3.975391	0.029463	14.579682	0.012365
0.3	5.810850	0.046977	22.314679	0.018934

For both the 0.3% and 0.6% concentration there is a noticeable increase in the pressure drop and decrease in the average fluid velocity. This is consistent with the observation made for the 0.1% concentration. Again, in order to assess the overall viability of the system at these lower flow rates it becomes necessary to consider the both the rate of removal of thermal energy and the effects on pumping requirements. To do this the average Nusselt number and Fanning friction factor are shown in Table 8 and Table 9 for 0.3% and 0.6% respectively.

Table 8: Average Nusselt Number and Fanning Friction Factor for 0.3% Nanofluid

Flow Rate (USGPM)	Bulk Media		Porously Filled Channels	
	Nu_{avg}	$f_{friction}$	Nu_{avg}	$f_{friction}$
0.1	43.3963	2.500008	68.0154	47.78706879
0.2	82.7374	1.118787	85.0909	23.50738401
0.3	88.5872	0.646079	87.2629	15.34306818

Table 9: Average Nusselt Number and Fanning Friction Factor for 0.6% Nanofluid

Flow Rate (USGPM)	Bulk Media		Porously Filled Channels	
	Nu_{avg}	$f_{friction}$	Nu_{avg}	$f_{friction}$
0.1	52.3447	2.533543237	74.5286	48.44388311
0.2	41.5898	1.14435628	90.6212	23.82841464
0.3	47.5103	0.657967505	106.6772	15.55396928

It can be seen that in both concentrations the Fanning friction factor is close on a per flow rate basis. This is likely as a result of the small changes in the fluid properties with the change in concentrations. However, there does exist a deviation in behaviour of the Nusselt number between the 0.3% and 0.6% concentrations when considering the bulk media. As the flow rate increases the 0.3% shows a corresponding increase in average Nusselt number, whereas the 0.6% concentration shows a decrease. This is possibly as a result of the ratio in change of fluid viscosity to thermal conductivity. As the fluid concentration increases the viscosity increases which inhibits the movement of fluid, and as such the convective mechanism. However, it is possible that the rate at which the effective thermal conductivity is changing is not proportional and is causing an overall reduction in the thermal enhancement. Similarly, to above the combination of the thermal performance and the pressure effects can be presented in the form of the thermal performance index. This index can be used in engineering design to make decisions regarding cost and performance. The index of performance as a function of flow rate is shown in Figure 10.

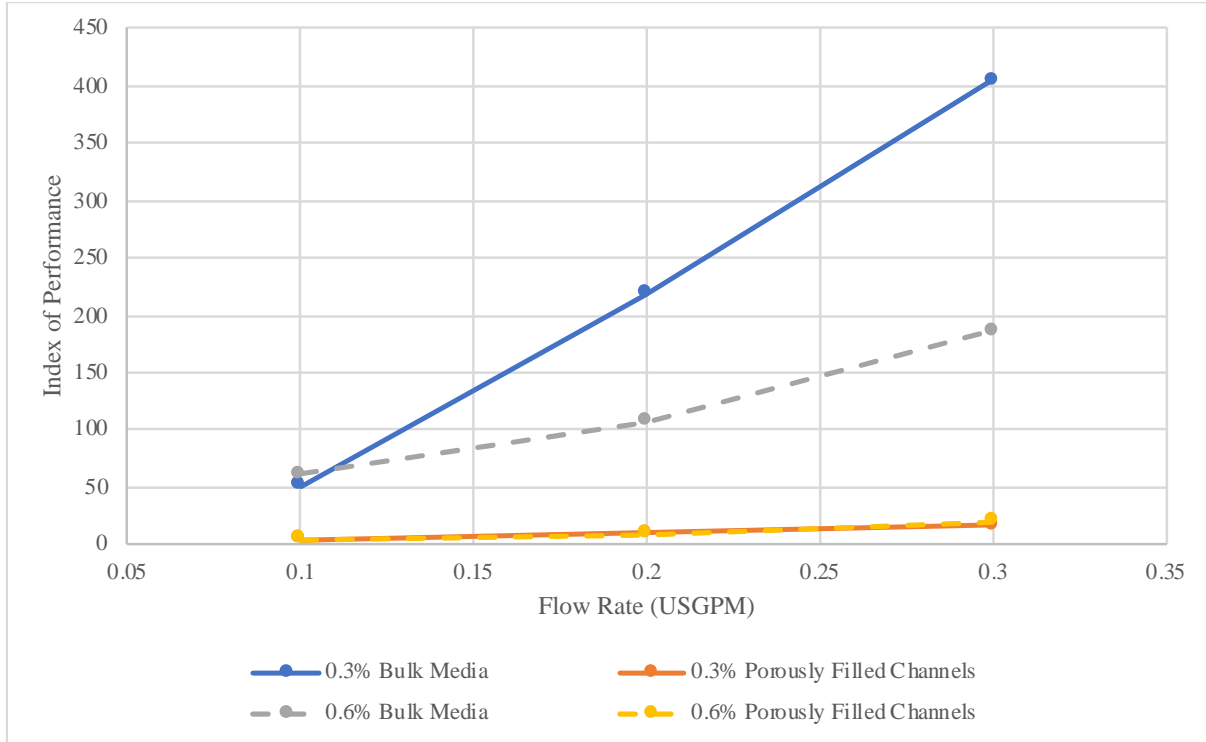


Figure 10: Index of Performance by Flow Rate for 0.3% and 0.6% Nanoparticle Concentration

When considering the flow rate of the system the following can then be said. The higher flow rates, above 0.3 USGPM should be avoided due the high Reynold's number and associated transitional flow which is caused. Further, when considering flow rate as the primary operating parameter it can be said that the highest possible flow rate is favourable for all concentration and geometries. The impact of the flow rate on the system is most clear in the bulk media samples which show rapid growth as flow rate increases.

4.2 Effect of Heat Flux on System Performance

Having established the effect which flow rate plays in the system performance it becomes necessary to determine how the various system configurations behave under different loading conditions. To simulate this the nominal inbound heat flux for the system was varied between $50000 \frac{W}{m^2}$, $75000 \frac{W}{m^2}$, and $100000 \frac{W}{m^2}$, corresponding to heat flux 1, heat flux2, and heat flux 3 respectively. The following considers a constant flow rate of 0.2 USGPM. The temperature distributions for the bulk and porously filled channels interacting with 0.1% Nanofluid are shown in Figure 11 (a) and (b) respectively.

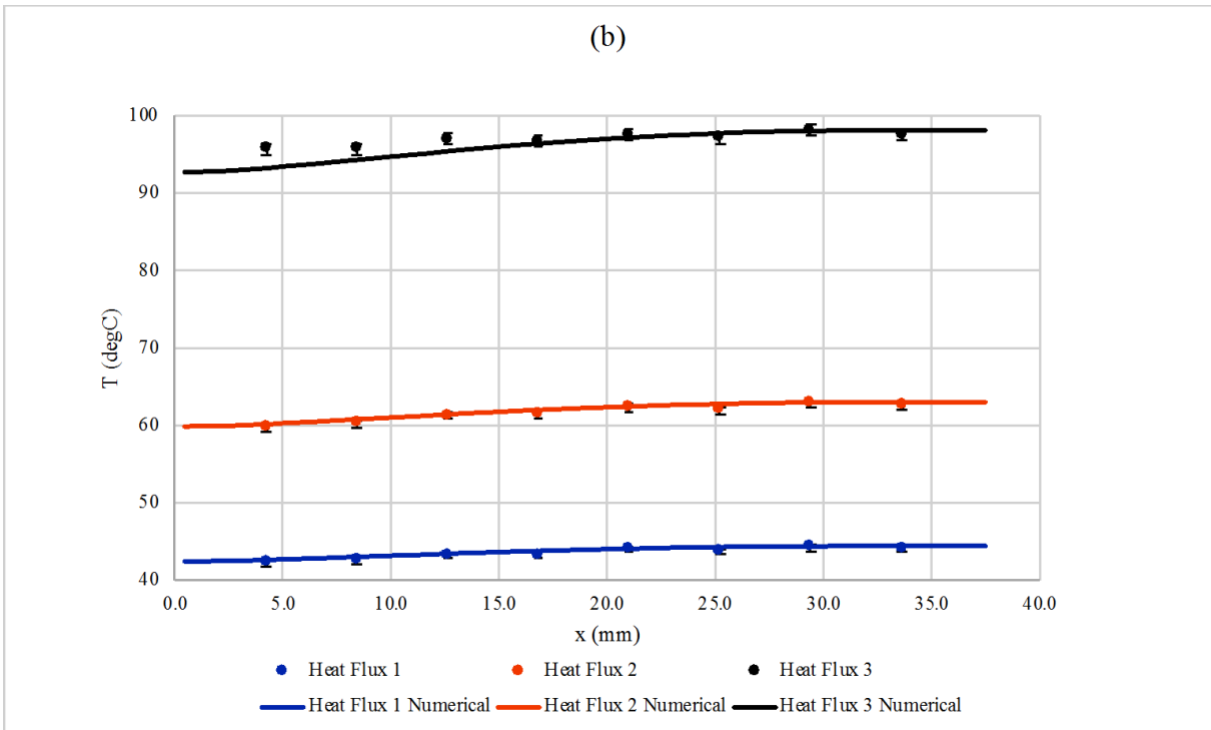
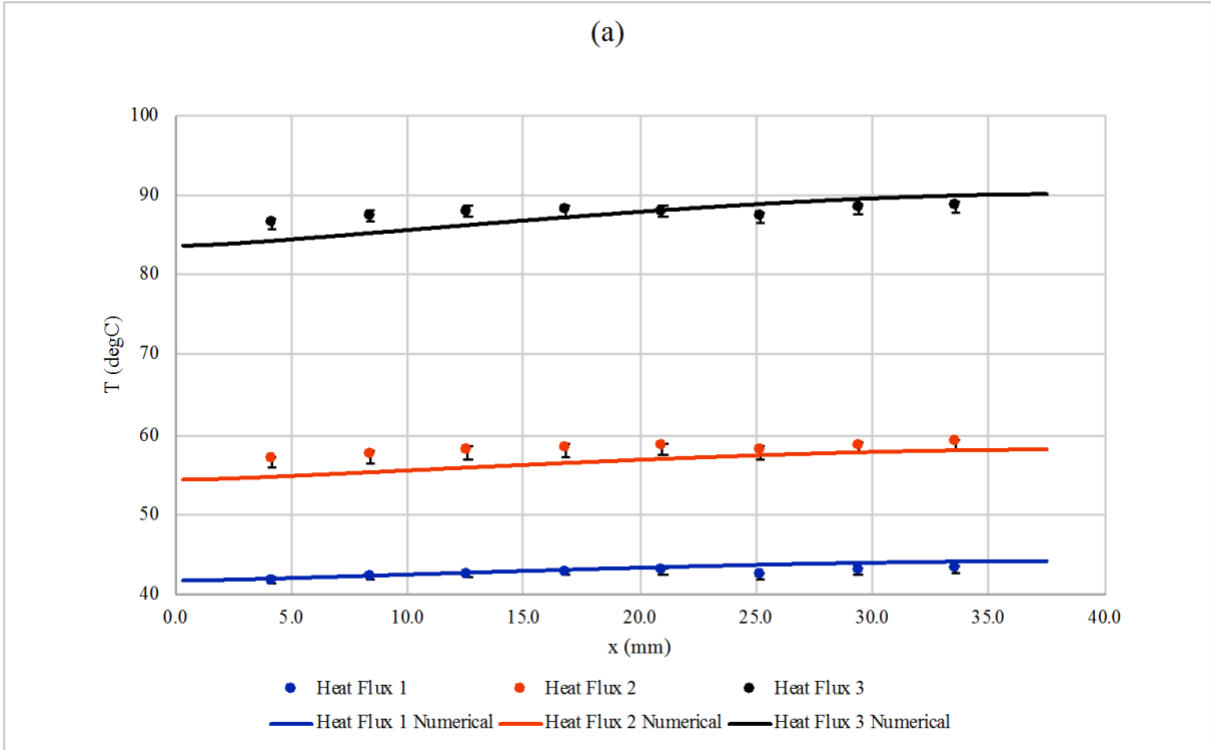


Figure 11: Temperature Distribution for (a) Bulk Media and (b) Porously Filled Channels Interacting with 0.1% Nanofluid

As is expected, as the inward heat flux is increased so too is the mean value of the temperature distribution. The temperature distribution for 0.3% and 0.6% Nanofluid are shown in Figure 12 and Figure 13.

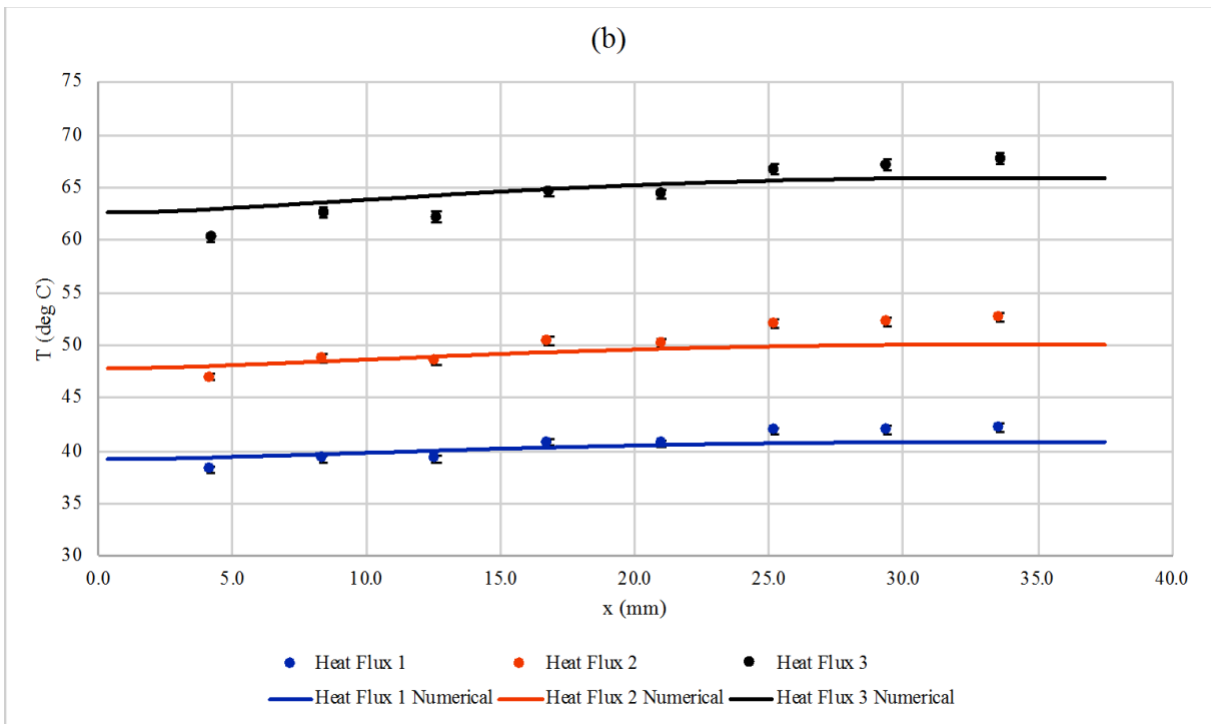
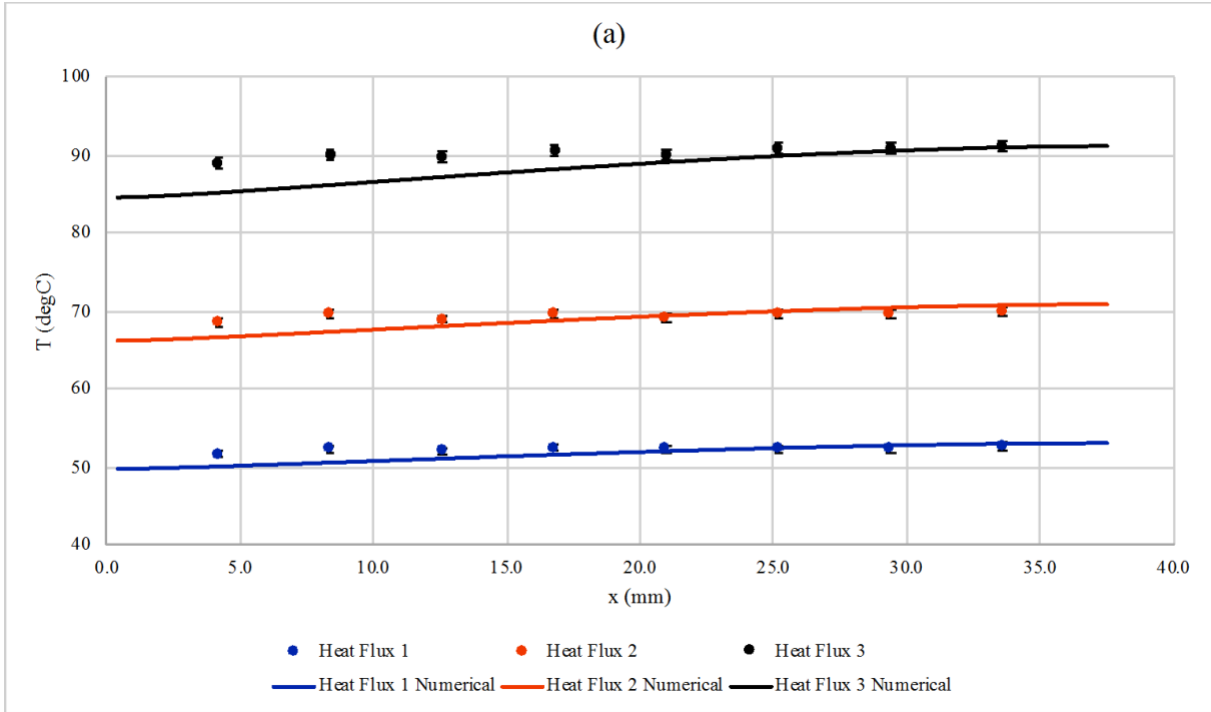


Figure 12: Temperature Distribution for (a) Bulk Media and (b) Porously Filled Channels Interacting with 0.3% Nanofluid

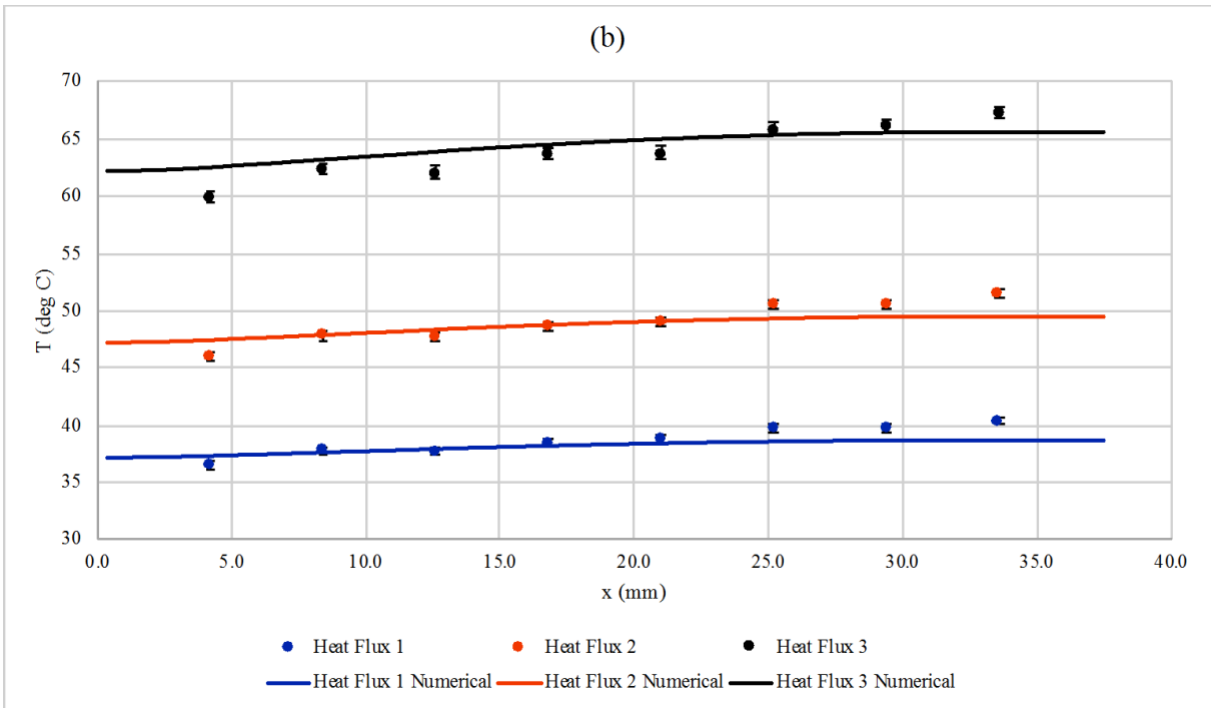
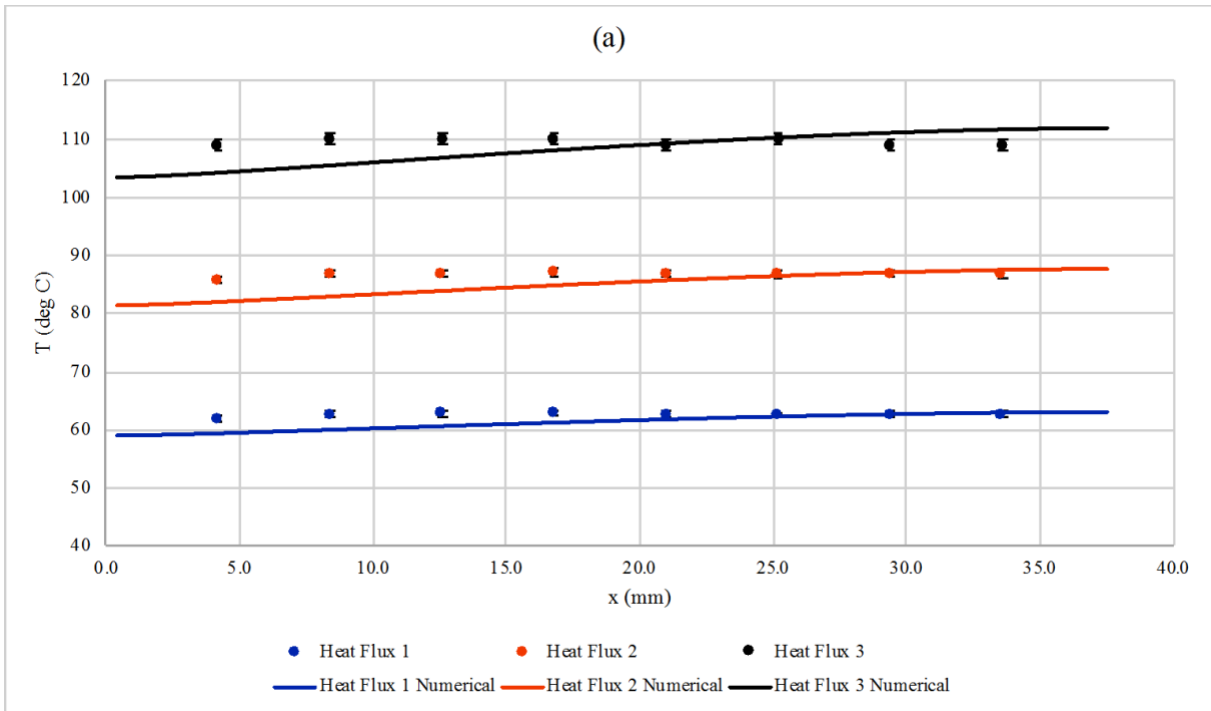


Figure 13: Temperature Distribution for (a) Bulk Media and (b) Porously Filled Channels Interacting with 0.6% Nanofluid

The same trend as a function of heat flux is observable across all three Nanofluid concentrations. This shows that whenever possible it is favourable to minimize the heat flux into the system. However, this is typically not a system parameter which can be freely mitigated. As such, the results show that there does not exist a critical heat flux within the present study which causes a change in the distribution of temperatures. To further assess the impact of heat flux on thermal performance the average Nusselt number is shown in Table 10 and Table 11 for bulk and porously filled channels respectively.

Table 10: Average Nusselt Number for Varied Heat Flux

Nominal Heat Flux $\left(\frac{W}{m^2}\right)$	Nanofluid Concentration (% by Volume)		
	0.1	0.3	0.6
50000	54.2658	82.7374	41.5898
75000	55.8067	83.2287	35.5390
100000	43.0832	81.3292	34.6764

Table 11: Average Nusselt Number for Porously Filled Channels

Nominal Heat Flux $\left(\frac{W}{m^2}\right)$	Nanofluid Concentration (% by Volume)		
	0.1	0.3	0.6
50000	58.4218	85.0909	90.6212
75000	48.4264	77.5265	83.9162
100000	36.2832	73.4356	76.9266

The results show a distinct decrease in the average Nusselt number between $50000 \frac{W}{m^2}$ and $75000 \frac{W}{m^2}$ apart from the 0.1% and 0.3% bulk media concentrations. It is possible that this deviation from the observed trend is as a result of experimental error in the measurement of the inbound heat flux as the source power fluctuates. As the Nusselt number is a function of the convective heat transfer coefficient, which is proportional to heat flux, it is contradictory to expectations that the average Nusselt number decrease as the inward heat flux increase. This contradictory result likely stems from the manipulation of the fluid's properties as the temperature gradient increases, causing a disagreement with the results anticipated in conventional thermal transport.

4.3 Effect of Nanoparticle Concentration on System Performance

The selection of a working fluid represents a critical stage when considering the design of a forced convection heat transfer system. In the present study three concentrations of Al₂O₃-water Nanofluid are considered for viability in heat transfer applications. When considering the effects of the fluid concentrations on the performance of the system it is crucial to consider the changes in both heat transfer and flow characteristics of the fluid. The fluid properties employed at present are treated as constants based on the work conducted by Ho et. al. [10]. In order to properly understand the exact effect which, the Nanofluid concentration has on the systems performance the heat flux and flow rate will be fixed at $50000 \frac{W}{m^2}$ and 0.2 USGPM respectively. The temperature distributions for all three concentrations of Nanofluid are shown for bulk media and porously filled channels in Figure 14 (a) and (b) respectively.

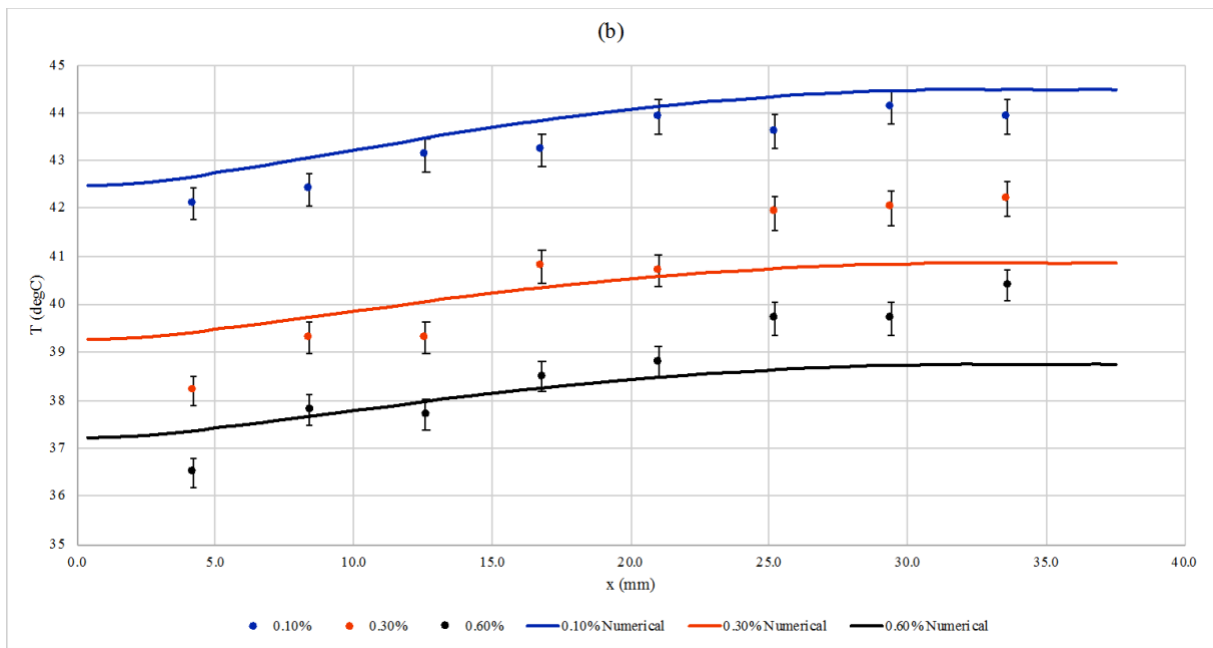
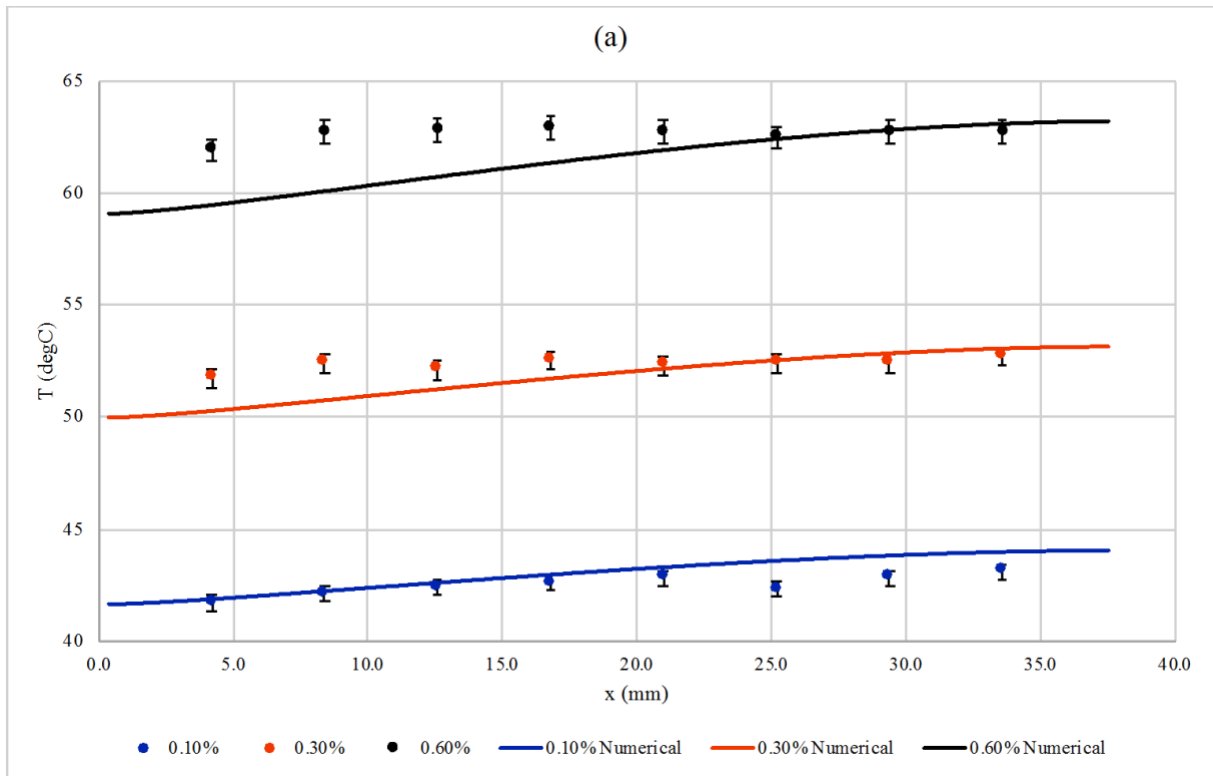


Figure 14: Temperature Distributions for (a) Bulk Porous Media and (b) Porously Filled Channels for All Nanofluid Concentrations

When comparing the results of the two separate geometries the trend associated with concentration is exactly the opposite between the two cases. For the bulk porous sample, the temperature

distribution can be seen to increase with the increasing Nanofluid concentration. Oppositely, the porously filled channel sample shows a decrease in temperature with the increasing Nanofluid concentration. It is likely that this occurs as a result of the reduced fluid velocity within the porously filled channels. Table 4, Table 6, and Table 7 show that the model including channels has a lower mean fluid velocity in all cases than that of the bulk porous media. It is likely that this reduced fluid flow allows more time for the Nanofluid to absorb thermal energy from the system before exiting and dissipating the energy to the atmosphere. Ultimately, as the system then approaches steady state there is then less residual energy at the heater interface. The purely thermal performance of the system is represented as a function of the strength of the convective heat transfer mechanism. This is quantified through use of the average Nusselt number. The average Nusselt number as a function of the concentration of the fluid for both geometries is shown in Figure 15.

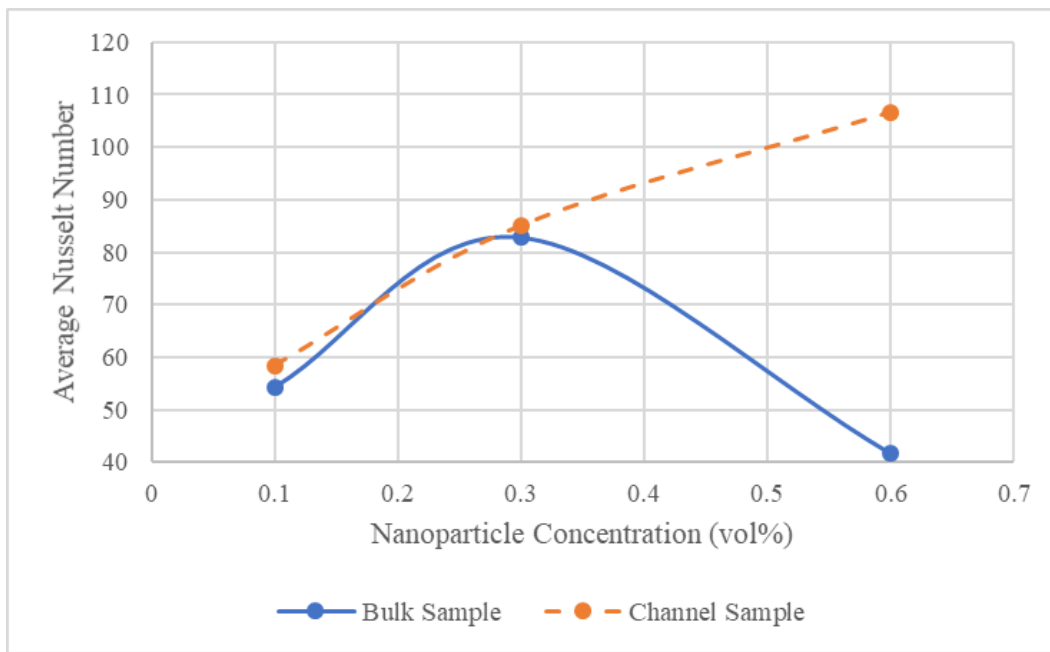


Figure 15: Average Nusselt Number Based on Nanofluid Concentration

When considering only the rate of removal of thermal energy there exists two distinct trends which exist based on Nanofluid concentration. When the porously filled channels are used the heat transfer continues to strengthen as the Nanofluid concentration is increased; with a notable decrease in the rate of change between 0.3% and 0.6%. When the bulk medium is considered there exists a clear optimum at a concentration of 0.3%. After this optimum is reached, increasing the

Nanofluid concentration appears to reduce the effectiveness of the heat transfer mechanism. Similar optima to this have been observed by Bayomy et. al. [51] when considering Nanofluid interactions with foam metals. The exact nature which drives these local optima still remains unexplained, but the above results do help to reinforce their existence. The concentration of 0.3% is consistent in both geometries with a change in the behaviour of the system. This commonality between both geometries also further reinforces the existence of a system dependant optimum. Due to the changes in fluid properties it is important to also compare the effects which the change in concentration has on the overall system performance. This is shown in the form of the index of performance again for a fixed flow rate of 0.2 USGPM and constant nominal heat flux of $50000 \frac{W}{m^2}$. The index of performance is shown for both geometries in Figure 16.

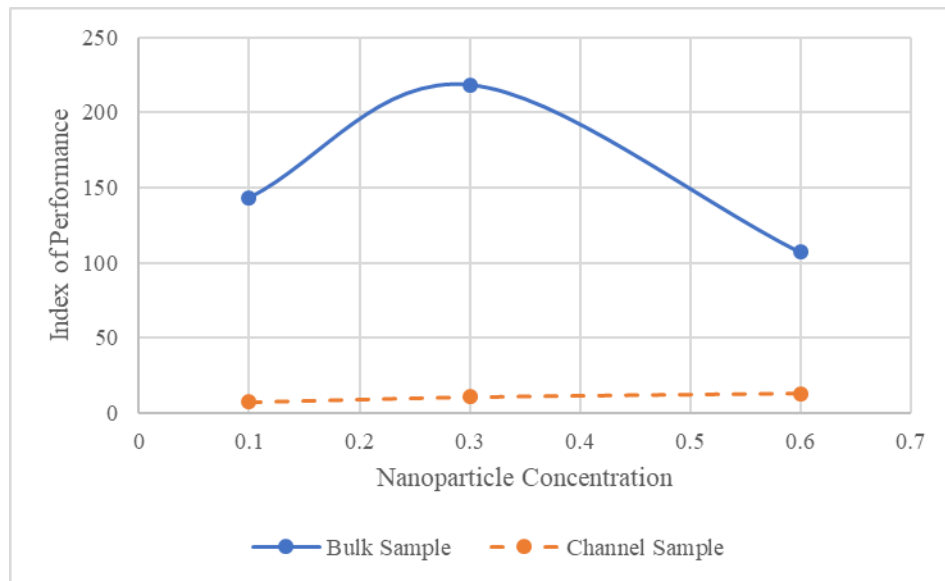


Figure 16: Effect of Nanofluid Concentration on Index of Performance

Similarly, to the local optimum which was observed when considering the average Nusselt number there exists a local optimum in the index of performance. However, when considering the index of performance, the bulk sample outperforms the porously filled channels. This is in contradiction to the average Nusselt number where it could be argued that the porously filled channels were favourable as they showed continuous growth for all Nanofluid concentrations. This dramatic difference between the porously filled channels and the bulk media for all concentrations is likely as a result of the interference to the flow from the solid walls.

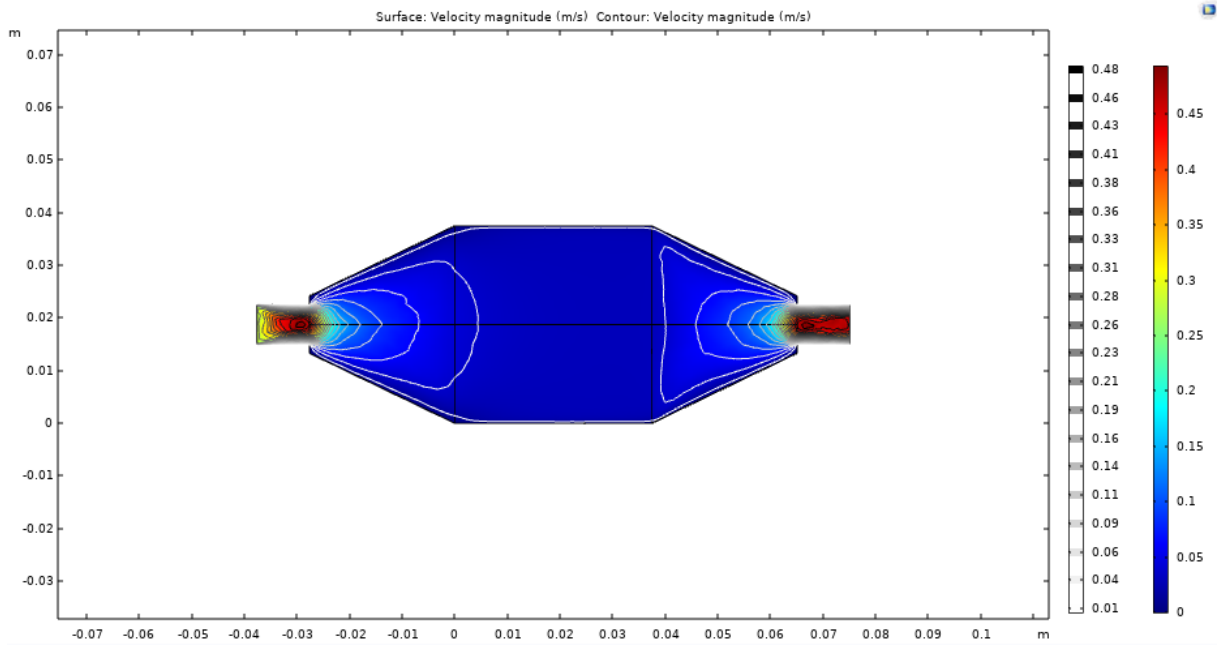
4.4 Effect of Channels on System Performance

The final aspect to consider when developing a thermal system is the use of either bulk porous media or porously filled channels. It was shown in section 4.3 that the average Nusselt number was higher for all Nanofluid concentrations interacting with the porously filled channels. However, when considering the index of performance, the porously filled channels performed poorly. Specifically, the average Nusselt number and index of performance for a constant concentration of 0.3% and a fixed flow rate and heat flux of 0.2 USGPM and $50000 \frac{W}{m^2}$ respectively are shown in Table 12.

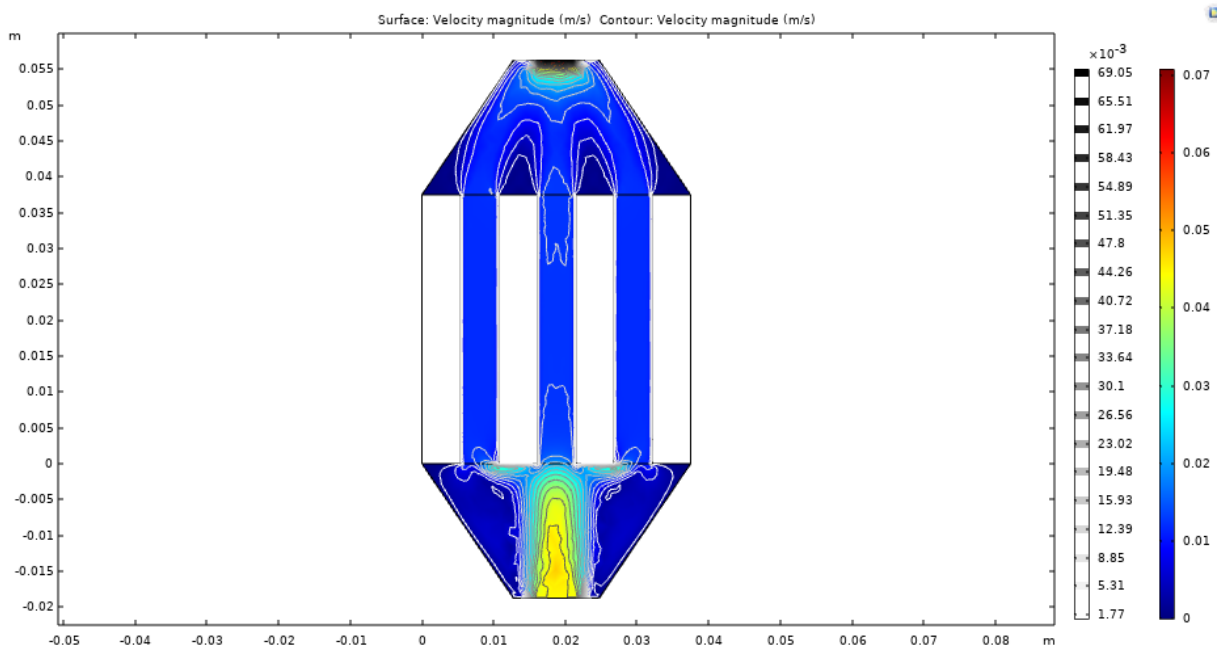
Table 12: Average Nusselt Number and Index of Performance for Bulk Media and Porously Filled Channels

Sample Type	Average Nusselt Number	Index of Performance
Bulk Media	82.7374	218.3644001
Porously Filled Channels	85.0909	10.68824406

It can be seen then that the difference between average Nusselt numbers when all conditions other than test sample are equal is 2.8%. However, the difference in index of performance between the two samples is equal to 95.1%. This dramatic reduction in overall system performance outweighs the slight gain in thermal performance which is observed. Section 4 shows us that the index of performance is a function of both Nusselt number, and the pumping power required to move the fluid through the system. It can then be seen from section 4.1 that the reason for this dramatically reduced index of performance is the dramatically higher pressure drop across the porously filled channel sample. To better understand the phenomena which causes this increase in pressure drop it becomes necessary to analyze the velocity distributions of the fluid through the system. The surface velocity distributions are shown in Figure 17 for (a) bulk media and (b) porously filled channels.



(a)



(b)

Figure 17: Velocity Profiles for (a) Bulk Media and (b) Porously Filled Channels

The surface velocity distributions show a tighter packing of constant speed contours. This indicates that as the fluid approaches the walls of the solid fins the fluid is forced to slow. To more closely understand the effects which the inclusion of channels has on the system, the velocity through the centre of the foam for both geometries is shown in Figure 18.

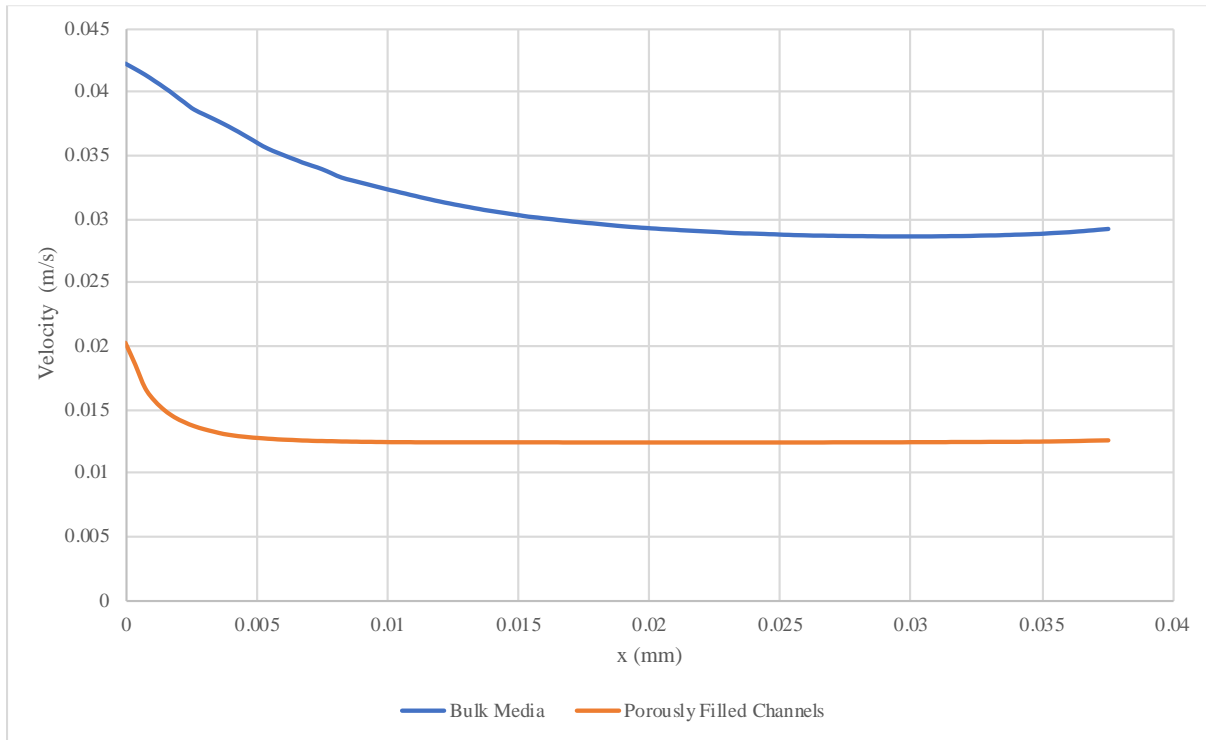
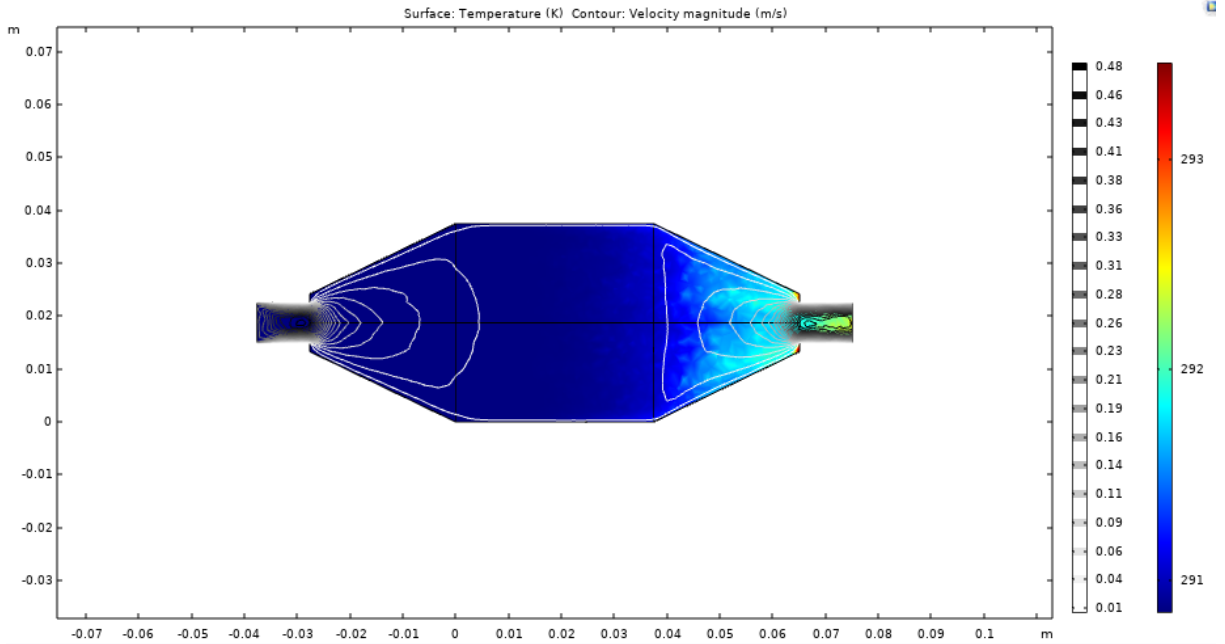
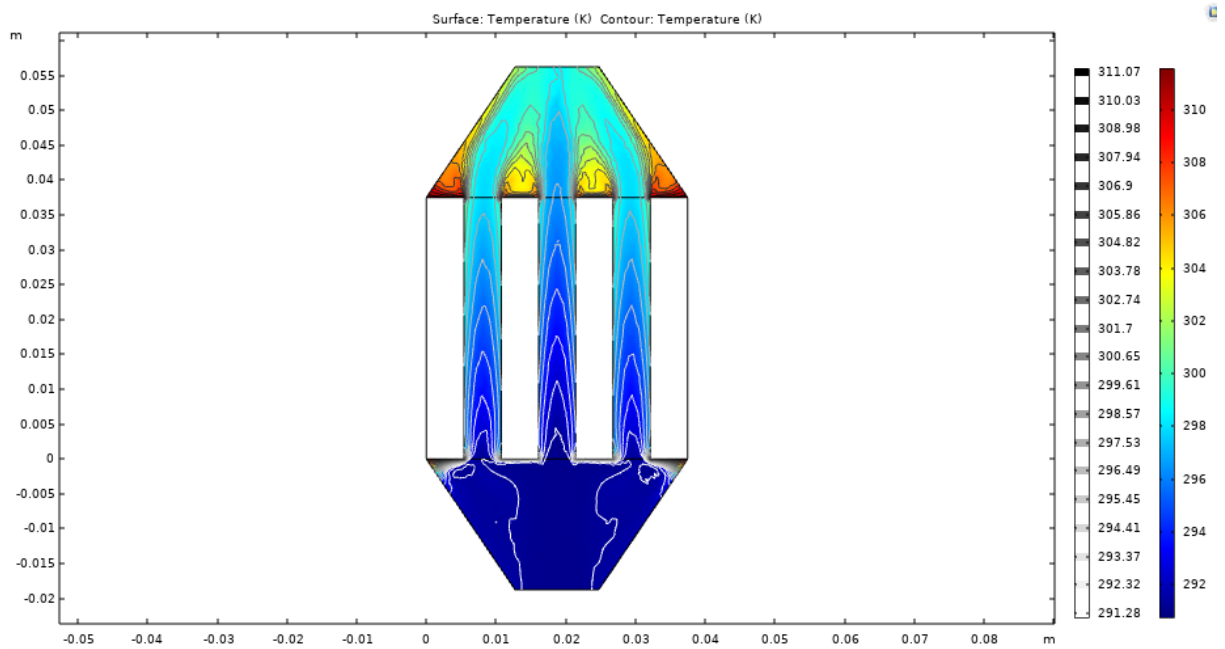


Figure 18: Velocity Profile Through Centre of the Test Sample

The plot shows a clear distinction between the bulk media and porously filled channels when considering the movement of the fluid through the sample. The first noticeable difference between the tests is the rate at which the velocity decreases as the fluid enters the system. In the porously filled channel test the velocity drops very quickly while the bulk media gradually decreases. This sudden decrease in fluid velocity which is present with the porously filled channel study explains the dramatically increased pressure drop present in the porously filled channel tests. Further, the velocity within the porously filled channels sample is generally lower than that within the bulk media. As the Fanning friction factor is a function of both pressure and velocity it becomes more clear as to why the porously filled channel model performed so poorly relative to that of the bulk media. Lastly, the fluid can be seen to begin accelerating more rapidly in the bulk media towards the exit of the sample when compared to the porously filled channel sample.



(a)



(b)

Figure 19: Plane Temperature Distribution for (a) Bulk Media and (b) Porously Filled Channels

(b)

Figure 19 shows the distribution of isothermal contours throughout the test section. It can be seen that in Figure 19 (b) the isothermal contours are much more tightly packed than those shown for the bulk media. This indicates that the temperature gradient throughout the sample is more drastic. This intensified temperature gradient helps in explaining the increased average Nusselt number observed within the porously filled channel samples. However, it can also be seen that as the fluid is interacting with the walls there exists a developing thermal boundary layer. In the bulk media sample this development of a boundary layer is insignificant, while in the porously filled channel the boundary layers develop very rapidly. In the outer two channels the boundary layers can even be seen as self-interfering. This implies that for the porously filled channels there will exist an optimal flow rate, after which, further increase in flow will reduce the system's performance. Further it can be seen that the centre channel has the lowest temperature of the three channels. This shows, as can be expected, that there exists a disparity in how the fluid fills the system as a result of the geometry. Namely, the fluid favours the centre channel which is in line with the inlet. These factors all indicate that when the power required to move the fluid through the porously filled channel sample, and the gradient of temperature are relevant design criteria, it is necessary to employ bulk media.

4.5 Applications of Results

The above information represents a total set of parameters which can be used in the design of any forced convection heat transfer system. It then becomes important to determine the engineering viability of the system from an application perspective. As the flat plate flow case studied in the present work is fairly general it then becomes possible to say that the theory contained herein can be applied to a wide variety of systems. The first example of these systems is the cooling of electronics. The experimental apparatus used herein mimics exactly the geometry of an intel i7 CPU. This makes the connection between this cooling technique and application in the electronics community evident. However, the above observed behaviour can be further extended to other heat transfer systems. One area in which there is growing interest is the cooling of bearings using foam metal heat sinks. The above results can be used to determine which design orientations and parameters are favourable for the operation of the particular system in question. Lastly, it is possible to extend the model and apply it wherein the objective is to use hot fluid to heat a cold plate.

5 Concluding Remarks and Future Work

The present work has successfully shown relationships between flow rate, heat flux, sample geometry, and Nanofluid concentration. The current study considered both numerically and experimentally derived results which showed good agreement to each other. To perform the numerical computations the empirical and numerical data obtained by Ho et. al. was used [8]- [11]. The results considered the effects of flow rate, inward heat flux, Nanofluid concentration, and system geometry. The Nanofluid concentrations considered were 0.1%, 0.3 %, and 0.6% by volume. The study considered both bulk porous media and porously filled channels. To determine the effectiveness of the system two parameters were used. The average Nusselt number was used to determine the strength of the convective mechanism present within a particular study. This value showed the performance of the system from a purely heat transfer driven perspective. The index of performance was used to evaluate the system as a whole including the pressure effects within the system.

5.1 Conclusions

The following major results can then be stated when considering the above study.

- COMSOL Multiphysics when combined with the Nanofluid properties provided by Ho et. al. [11] represents a viable way to simulate the interactions between Nanofluids and highly permeable foam metals.
- The maximum relative error present between the numerical and experimental results was found to be 4.3%.
- When considering the flow rate of the Nanofluid through the system an increased flow rate always tended to yield an improvement in the thermal performance index until the flow transitioned beyond the laminar regime.
- An increase in heat flux produced a directly associated increase in temperature distribution. However, it did not produce a proportional increase in average Nusselt number as would normally be expected.
- Altering the Nanofluid concentration within the bulk porous media shows profound effect on both the average Nusselt number and Index of Performance.

- For the bulk porous media, a local optimum was observed at 0.3% concentration by volume. After the local optimum the Nanofluid began to inhibit the performance of the system
- Increasing the Nanofluid concentration within the porously filled channel test tended to always increase the performance of the system.
- At a concentration of 0.3% Nanofluid by volume it was observed that the rate at which the thermal performance improved was decreased.
- When porously filled channels were used it was shown that for all Nanofluid concentrations a higher average Nusselt number was obtained
- The maximum average Nusselt numbers are 82.7 at a concentration of 0.3% Nanofluid and 106.7 at a concentration of 0.6% Nanofluid for the bulk media and porously filled channels respectively.
- The index of performance for porously filled channels was lower than all cases of that for bulk media.
- The maximum values for the calculated index of performance are 218.4 at a concentration of 0.3% and 13.2 at a concentration of 0.6% for bulk media and porously filled channels.
- When considering only the strength of the convective mechanism in a design scenario it can then be said, based off of average Nusselt number, that a system operating with 0.6% Nanofluid and porously filled channels should be selected.
- If the system pumping power is a necessary design factor, then it can be said that a system should employ 0.3% Nanofluid with bulk porous media.

5.2 Future Work

To better understand the nature of the thermal and fluid transport phenomena which are taking place in the present study it is important to continue with a focussed direction. The following are areas related to the present which require further specific study:

- Further developed formulation for thermal and fluidic entry and exit region behaviour for both Nanofluid and foam metals.
- A more general relationship for the Nanofluid properties used which is not a constant but rather a function of local system conditions including temperature and pressure.

- A more detailed understanding of the forces which drive the enhancement caused by Nanofluid to allow more accurate prediction of the fluid properties.
- The development of an approach to model the realistic geometry of the foam metals which does not require the destruction of the sample allowing for comparison between general Navier-Stokes flow, present statistical and numerical models, and experimental results.
- Refinement of the system used for the measurement of inward heat flux into the experimental system.

References

- [1] H. Darcy, *Les Fontaines Publiques de la Ville de Dijon*, Paris, France: ATLAS, 1856.
- [2] A. Kopanidis, A. Theodorakakos, E. Gavaises and D. Bouris, "3D numerical simulation of flow and conjugate heat transfer through a pore scale model of high porosity open cell metal foam," *International Journal of Heat and Mass Transfer*, vol. 53, pp. 2539-2550, 2010.
- [3] P. Ranut, E. Nobile and L. Mancini, "High resolution microtomography-based CFD simulation of flow and heat transfer in aluminum metal foams," *Applied Thermal Engineering*, vol. 86, no. 1-2, pp. 230-240, 2014.
- [4] D. Andrea, K. K. Bodla, L. Rossetto and S. V. Garimella, "Numerical investigation of pressure drop and heat transfer through reconstructed metal foams and comparison against experiments," *International Journal of Heat and Mass Transfer*, vol. 88, pp. 508-515, 2015.
- [5] C. Xu, Y. Mao and Z. Hu, "Numerical study of pore-scale flow and noise of an open cell metal foam," *Aerospace Science and Technology*, Vols. 82-83, pp. 185-198, 2018.
- [6] N. Dukhan, O. Bagci and M. Ozdemir, "Metal foam hydrodynamics: Flow regimes from pre-Darcy to turbulent," *International Journal of Heat and Mass Transfer*, vol. 77, pp. 114-123, 2014.
- [7] R. Dyga and M. Płaczek, "Selected problems of gas-liquid flow through the channels filled with metal foams," *Transport in Porous Media*, vol. 73, no. 2, pp. 233-254, 2017.
- [8] C. Ho, M. Chen and Z. Li, "Numerical Simulation of Natural Convection of Nanofluid In a Square Enclosure: Effects Due to Uncertainties of Viscosity and Thermal Conductivity," *International Journal of Heat and Mass Transfer*, vol. 51, no. 17, pp. 4506-4516, 2008.
- [9] C. Ho, L. Wei and Z. Li, "An Experimental Investigation of Forced Convective Cooling Performance of a Microchannel Heat Sink with Al₂O₃/Water Nanofluid," *Applied Thermal Engineering*, vol. 30, no. 2-3, pp. 96-103, 2009.
- [10] C. Ho, W. Liu, Y. Chang and C. Lin, "Natural Convection Heat Transfer of Alumina-Water Nanofluid in Vertical Square Enclosures: An Experimental Study," *International Journal of Thermal Sciences*, vol. 49, no. 8, pp. 1345-1353, 2010.

- [11] C. Ho and W. Chen, "An Experimental Study on Thermal Performance of Al₂O₃/Water Nanofluid in a Minichannel Heat Sink," *Applied Thermal Engineering*, vol. 50, no. 1, pp. 516-522, 2013.
- [12] A. Arefmanesh and M. Mahmoodi, "Effects of uncertainties of viscosity models for Al₂O₃water nanofluid on mixed convection numerical simulations," *International Journal of Thermal Sciences*, vol. 50, pp. 1706-1719, 2011.
- [13] M. Sheikholeslami and M. K. Sadoughi, "Numerical modeling for Fe₃O₄-water nanofluid flow in porous medium considering MFD viscosity," *Journal of Molecular Liquids*, vol. 242, pp. 255-264, 2017.
- [14] S. Etaig, R. Hasan and N. Perera, "A New Effective Viscosity Model for Nanofluids," *International Journal of Numerical Methods for Heat and Fluid Flow*, vol. 28, no. 3, pp. 571-583, 2018.
- [15] O. Soltani and M. Akbari, "Effects of temperature and particles concentration on the dynamic viscosity of MgO-MWCNT/ethylene glycol hybrid nanofluid: Experimental study," *Physica E*, vol. 84, pp. 564-570, 2016.
- [16] G. M. Moldoveanu, A. A. Minea, M. Iacob, C. Ibanescu and M. Danu, "Experimental study on viscosity of stabilized Al₂O₃, TiO₂ nanofluids and their hybrid," *Thermochimica Acta*, vol. 659, pp. 203-212, 2018.
- [17] C. T. Hsu, P. Cheng and K. W. Wong, "Modified Zehner-Schlunder models for stagnant thermal conductivity of porous media," *International Journal of Heat and Mass Transfer*, vol. 37, no. 17, pp. 2751-2759, 1994.
- [18] A. Bhattacharya, V. V. Calmidi and R. L. Mahajan, "Thermophysical properties of high porosity metal foams," *International Journal of Heat and Mass Transfer*, vol. 45, pp. 1017-1031, 2002.
- [19] K. Boomsma and D. Poulikakos, "On the effective thermal conductivity of a three-dimensionally structured fluid-saturated metal foam," *International Journal of Heat and Mass Transfer*, vol. 44, pp. 827-836, 2001.
- [20] Z. Dai, K. Nawaz, Y. G. Park, J. Bock and A. M. Jacobi, "Correcting and Extending the Boomsma-Poulikakos Effective Thermal Conductivity Model for Three-Dimensional Fluid-

- Saturated Metal Foams," *International Communications in Heat and Mass Transfer*, vol. 37, pp. 575-580, 2010.
- [21] K. Boomsma and D. Poulikakos, "Corrigendum for the paper: K. Boomsma, D. Poulikakos, "On the effective thermal conductivity of a three-dimensionally structured fluid-saturated metal foam" [International Journal of Heat and Mass Transfer, 44 (2001) 827–836]," *International Journal of Heat and Mass Transfer*, vol. 54, pp. 746-748, 2011.
- [22] D. A. Nield, A. V. Kuznetsov and M. Xiong, "Thermally developing forced convection in a porous medium: parallel plate channel with walls at uniform temperature, with axial conduction and viscous dissipation effects," *International Journal of Heat and Mass Transfer*, vol. 46, pp. 643-651, 2003.
- [23] A. V. Kuznetsov and D. A. Nield, "Forced Convection with Slip-Flow in a Channel Occupied by a Hyperporous Medium Saturated by a Rarefied Gas," *Transport in Porous Media*, vol. 76, no. 3, pp. 345-362, 2009.
- [24] K. Hooman and A. Haji-Sheikh, "Analysis of heat transfer and entropy generation for a thermally developing Brinkman–Brinkman forced convection problem in a rectangular duct with isoflux walls," *International Journal of Heat and Mass Transfer*, vol. 50, pp. 4180-4194, 2007.
- [25] D. Vijay, P. Goetze, R. Wulf and U. Gross, "Homogenized and pore-scale analyses of forced convection through open cell foams," *International Journal of Heat and Mass Transfer*, vol. 123, pp. 787-804, 2018.
- [26] Z. G. Xu, J. Qin, X. Zhou and H. J. Xu, "Forced convective heat transfer of tubes sintered with partially-filled gradient metal foams (GMFs) considering local thermal non-equilibrium effect," *Journal of Applied Thermal Engineering*, vol. 137, pp. 101-11, 2018.
- [27] A. Gandomkar and K. E. Gray, "Local thermal non-equilibrium in porous media with heat conduction," *International Journal of Heat and Mass Transfer*, vol. 124, pp. 1212-1216, 2018.
- [28] S. Chen, "Simulation of conjugate heat transfer between fluid-saturated porous media and solid wall," *International Journal of Thermal Sciences*, vol. 124, pp. 477-483, 2018.

- [29] L. Gong, Y. Li, Z. Bai and M. Xu, "Thermal performance of micro-channel heat sink with metallic porous/solid compound fin design," *Journal of Applied Thermal Engineering*, vol. 137, pp. 288-295, 2018.
- [30] A. Bhattacharya and R. L. Mahajan, "Finned Metal Foam Heat Sinks for Electronics Cooling in Forced Convection," *Journal of Electronic Packaging*, vol. 124, no. 3, pp. 155-163, 2002.
- [31] K. Boomsma, D. Poulikakos and F. Zwick, "Metal foams as compact high performance heat exchangers," *Mechanics of Materials*, vol. 35, pp. 1161-1176, 2003.
- [32] G. Hetsroni, M. Gurevich and R. Rozenblit, "Metal Foam Heat Sink for Transmission Window," *International Journal of Heat and Mass Transfer*, vol. 48, pp. 3793-3803, 2005.
- [33] C. Y. Zhao, T. Kim, T. J. Lu and H. P. Hodson, "Thermal Transport in High Porosity Cellular Metal Foams," *Journal of Thermophysics and Heat Transfer*, vol. 18, no. 3, pp. 309-318, 2004.
- [34] J.-S. Noh, K. B. Lee and C. G. Lee, "Pressure loss and forced convective heat transfer in an annulus filled with aluminum foam," *International Communications in Heat and Mass Transfer*, vol. 33, pp. 434-444, 2006.
- [35] S. Mancin and L. Rossetto, "An Assessment on Forced Convection in Metal Foams," in *Journal of Physics: Conference Series 395*, Poitiers, France, 2012.
- [36] X. H. Yang, J. X. Bai, H. B. Yan, J. J. Kuang, T. J. Lu and T. Kim, "An Analytical Unit Cell Model for the Effective Thermal Conductivity of High Porosity Open-Cell Metal Foams," *Transport Phenomena in Prous Media*, vol. 102, pp. 403-426, 2014.
- [37] N. Dukhan, A. A.-R. Muntadher and A. S. Suleiman, "Fluid temperature measurements inside metal foam and comparison to Brinkman–Darcy flow convection analysis," *International Journal of Heat and Mass Transfer*, vol. 67, pp. 887-884, 2013.
- [38] S. Mancin, C. Zilio, A. Diani and L. Rossetto, "Air forced convection through metal foams: Experimental results and modeling," *International Journal of Heat and Mass Transfer*, vol. 62, pp. 112-123, 2013.
- [39] N. Dukhan, O. Bagci and M. Ozdemir, "Thermal development in open-cell metal foam: An experiment with constant wall heat flux," *International Journal of Heat and Mass Transfer*, vol. 85, pp. 852-859, 2015.

- [40] E. Fleming, S. Wen, L. Shi and A. K. da Silva, "Experimental and theoretical analysis of an aluminum foam enhanced phase change thermal storage unit," *International Journal of Heat and Mass Transfer*, vol. 82, pp. 273-281, 2015.
- [41] O. Bagci, N. Dukhan and L. A. Kavurmacioglu, "Forced-Convection Measurements in the Fully Developed and Exit Regions of Open-Cell Metal Foam," *Transport Phenomena in Porous Media*, vol. 109, pp. 513-526, 2015.
- [42] S. Chen, W. Gong and Y. Yan, "Conjugate natural convection heat transfer in an open-ended square cavity partially filled with porous media," *International Journal Heat and Mass Transfer*, vol. 124, pp. 368-380, 2018.
- [43] H. Xu, L. Gong, S. Huang and M. Xu, "Flow and heat transfer characteristics of nanofluid flowing through metal foams," *International Journal of Heat and Mass Transfer*, vol. 83, pp. 399-407, 2015.
- [44] M. Ameri, M. Amani and P. Amani, "Thermal performance of nanofluids in metal foam tube: Thermal dispersion model incorporating heterogeneous distribution of nanoparticles," *Journal of Advanced Powder Technology*, vol. 28, pp. 2747-2755, 2017.
- [45] A. Karimi and M. Afrand, "Numerical study on thermal performance of an air-cooled heat exchanger: Effects of hybrid nanofluid, pipe arrangement and cross section," *Journal of Energy Conversion and Management*, vol. 164, pp. 615-628, 2018.
- [46] M. Nazari, M. Ashouri, M. H. Kayhani and A. Tamayol, "Experimental study of convective heat transfer of a nanofluid through a pipe filled with metal foam," *International Journal of Thermal Sciences*, vol. 88, pp. 33-39, 2015.
- [47] H. J. Jouybari, S. Saedodin, A. Zamzajian, M. E. Nimvari and S. Wongwises, "Effects of porous material and nanoparticles on the thermal performance of a flat plate solar collector: An experimental study," *Journal of Renewable Energy*, vol. 114, pp. 1407-1418, 2017.
- [48] M. H. Buschmann, R. Azizian, T. Kempe, J. E. Julia, R. Martinez-Cuenca, B. Sunden, Z. Wu, A. Seppala and T. Ala-Nissila, "Correct Interpretation of Nanofluid Convective Heat Transfer," *International Journal of Thermal Sciences*, vol. 129, pp. 504-531, 2018.

- [49] J. Akshay, J. J. Aswin, J. Jobin and B. Rajesh, "Enhancement of thermal performance of a loop heat pipe using alumina water nanofluid : An experimental investigation," in *IOP Conference Series: Material Science Engineering* 396, 2018.
- [50] A. Bayomy, M. Saghir and T. Yousefi, "Electronic Cooling Using Water Flow in Aluminum Metal Foam Heat Sink: Experimental and Numerical Approach," *International Journal of Thermal Sciences*, vol. 109, pp. 182-200, 2016.
- [51] A. Bayomy and M. Saghir, "Experimental Study of Using Al₂O₃ Water Nanofluid Flow Through Aluminum Foam Heat Sink: Comparisson with Numerical Approach," *International Journal of Heat and Mass Transfer*, vol. 107, pp. 181-203, 2016.
- [52] A. Bayomy and M. Saghir, "Experimental and Numerical Study of the Heat Transfer Characteristics of Aluminum Metal Foam (With/Without Channels) Subjected to Steady Water Flow," *Journal of Science and Technology*, vol. 25, no. 1, pp. 221-246, 2017.
- [53] M. Z. Saghir, C. A. Welsford, P. Thanapathy, A. M. Bayomy and C. Delisle, "Experimental Measurements and Numerical Computation of Nano Heat Transfer Enhancement Inside a Porous Material," *Journal of Thermal Science and Engineering Applications*, vol. 12, 2019.
- [54] C. A. Welsford, A. M. Bayomy and M. Z. Saghir, "Role of metallic foam in heat storage in the presence of nanofluid and microencapsulated phase change material," *Thermal Science and Engineering Progress*, vol. 7, pp. 61-69, 2018.
- [55] B. Battleson, "Duocel Aluminum Foam," ERG Aerospace, 2019. [Online]. Available: <http://ergaerospace.com/materials/duocel-aluminum-foam/>.
- [56] "Buy Al₂O₃-monodisperse spherical nanoparticles in Aqueous media | Al₂O₃-monodisperse spherical nanoparticles in Aqueous media online: MKNano.com," Mknano.com, 2019. [Online]. Available: [https://www.mknano.com/Nanoparticles/Single-Element-Oxides/Aluminum-Oxide-Nanopowder/Al₂O₃-monodisperse-spherical-nanoparticles-in-Aqueous-media](https://www.mknano.com/Nanoparticles/Single-Element-Oxides/Aluminum-Oxide-Nanopowder/Al2O3-monodisperse-spherical-nanoparticles-in-Aqueous-media).
- [57] comsol, "COMSOL Multiphysics Modeling Software," Comsol, 2019. [Online]. Available: <https://www.comsol.com>. [Accessed June 2019].